Geologica Acta, Vol.16, Nº 2, June 2018, 125-148
DOI: 10.1344/GeologicaActa2018.16.2.2

geologica acta

C and O stable isotopes and rare earth elements in the Devonian carbonate host rock of the Pivehzhan iron deposit, NE Iran

P. NAJAFZADEH TEHRANI[1] A.A. CALAGARI[1] F. VELASCO ROLDAN[2] V. SIMMONDS[3] K. SIAHCHESHM[1]

[1]Department of Earth Sciences, Faculty of Natural Sciences, University of Tabriz
5166616471,Tabriz, Iran. Najafzadeh Tehrani E-mail: parvin_tehranii@yahoo.com Tel: +98-41-33392699
Fax: +98-41-33392703

[2]Departamento de Mineralogía y Petrología, Facultad de Ciencia y Tecnología, Universidad del País Vasco
UPV/EHU, 48080 Bilbao, Spain. E-mail: francisco.velasco@ehu.es

[3]Research Institute for Fundamental Sciences, University of Tabriz
5166876393, Tabriz, Iran. E-mail: simmonds_vartan@yahoo.com.uk

ABSTRACT

The Pivehzhan iron deposit is located at about 80km southwest of Mashhad, NE Iran. It occur within the Devonian carbonates as lenticular and massive bodies, as well as veinlets of magnetite and iron sulphides, transformed to goethite and haematite by weathering process. The hydrothermal calcite is the most important gangue mineral, which is observed in the form of veins/veinlets and open-space filling. The iron ores are accompanied by some minor elements such as Mn, Ti, Cr, and V and negligible amounts of Co and Ni. The distribution pattern of Rare Earth Elements (REEs) normalized to Post Archean Australian Shale (PAAS), which is characterized by the upward convex, as well as the positive Eu anomalies indicate the activity of reduced and acidic hydrothermal fluids. The negative Ce anomalies of host carbonates, although slight, point to the dominance of anoxic conditions during interaction with hydrothermal fluids.

The hydrothermal calcite and quartz coexisting with the iron minerals contain principally fluid, which were homogenized into a liquid phase. The Homogenization Temperature (T_H) and the salinity of the analysed fluid inclusions range from 129°C to 270°C and from 0.4wt.% to 9.41wt.% NaCl eq., respectively. The $\delta^{13}C_{PDB}$ and $\delta^{18}O_{SMOW}$ values range from -2.15‰ to -5.77‰ (PeeDee Belemnite PDB standard) and from +19.87‰ to +21.64‰ (Standard Mean Ocean Water SMOW standard) in hydrothermal calcite veinlets occurring with iron minerals, and from -0.66‰ to -4.37‰ (PDB) and from +15.55‰ to +20.14‰ (SMOW) within the host carbonates, respectively.

The field relations and petrographic examination along with geochemical and isotopic considerations indicate that the Pivehzhan iron deposit was formed through replacement processes by reducing and acid fluids containing light carbon and oxygen isotopes. Variations in the physico-chemical conditions of hydrothermal fluids and their interaction with carbonates were the most effective mechanisms in the formation of this iron deposit. The potential source of iron was probably the basement magmatic rocks from which iron was leached by hydrothermal solutions.

KEYWORDS | **REE geochemistry. Carbonate host rocks. C and O stable isotopes. Pivehzhan. Iron.**

INTRODUCTION

Stable isotopes studies, mineral chemistry, and geochemistry of Rare Earth Elements (REEs) are three common methods used for constraining the mode of ore formation. Investigation of C and O isotopic composition in carbonate rocks and hydrothermal calcite is one of them. It has been used to investigate the origin of ore-forming fluids in metallic deposits (Zheng and Hoefs, 1993; Fernández-Nieto *et al.*, 2003; Torres-Ruiz, 2006; Taofa *et al.*, 2011; Zhou *et al.*, 2014). Additionally, geochemistry of REEs in carbonate host rocks of metallic deposits can be used to recognize the ancient sedimentary environment of the host rocks and the physico-chemical conditions of the ore forming fluids. The relative distribution of REEs in marine sediments indicates the presence of various hydrothermal fluids with different alkalinity and oxygen fugacity, which have been mixed with sea water within the depositional basin (Piepgras and Jacobsen, 1992; Bertram and Elderfield, 1993; Greaves *et al.*, 1999; Kamber *et al.*, 2004; Chen *et al.*, 2006; Feng *et al.*, 2009; Kim *et al.*, 2012; Hu *et al.*, 2014; Franchi *et al.*, 2015). Furthermore, variations in the concentrations of REEs and redox-sensitive trace elements are important in reconstructing the redox condition and mixing of fluids during the precipitation of marine carbonates (Jiang *et al.*, 2007). The iron deposits in the southwest of the city of Mashhad, NE Iran, occurred in separate ores within the Devonian carbonate rocks (Wauschkuhn *et al.*, 1984). Ancient workings, slags, and one old iron furnace indicate a long history of mining in this area (Wauschkuhn *et al.*, 1984). Pivehzhan iron ores include magnetite and iron sulphides (pyrite and pyrrhotite), transformed to goethite and haematite by weathering processes(Najafzadeh Tehrani *et al.*, 2016a). So far, no thorough investigation concerning the geochemistry and genesis of this deposit has been conducted. In the present study, the origin of hydrothermal fluids involved in the formation of this deposit will be discussed by focusing on the geochemical composition and mineral chemistry of the ore minerals, as well as considering the C and O stable isotopes in the hydrothermal calcite veinlets and host carbonates, beside the fluid inclusion data obtained from of the hydrothermal calcite and quartz veins. Meanwhile, the paleo-environment of formation of the host carbonates and their post-depositional diagenetic and metamorphic effects will be discussed based on the distribution pattern of REEs. Finally, the Eh and pH of the late ore-forming fluids and their relationship with the primary mineralization and host rocks will be considered.

GEOLOGY

Regional geology

The Pivehzhan iron deposit is located ~80km southwest of Mashhad, NE Iran. According to the structural zonation of Iran (Nabavi, 1976; Alavi, 1992). The study area lies in the South of the Binaloud Zone, East of the Alborz-Azarbidjan Zone (Fig. 1). Structural units in this region are either single thrust sheets or duplexes (Alavi, 1992). Due to its peculiar geologic situation, the Binaloud Zone is formed by a relatively thick sequence of sedimentary, metamorphic and volcanic rocks, and is affected by three generations of thrust faults striking toward the southwest (Fig. 2A). The overall strike of the sedimentary formations is NW-SE, which corresponds to the general trend of the Alpine orogeny in Iran (Alavi, 1992). The main stage of deformation occurred in two phases (Lammerer *et al.*, 1983; Alavi, 1992). The first phase, characterized by strong folding and weak regional metamorphism, took place during the late Variscan-early Kimmerian (Middle Jurassic) and the second phase, occurred during the Alpine orogeny, when folding was accompanied by volcanic activity (Lammerer *et al.*, 1983).

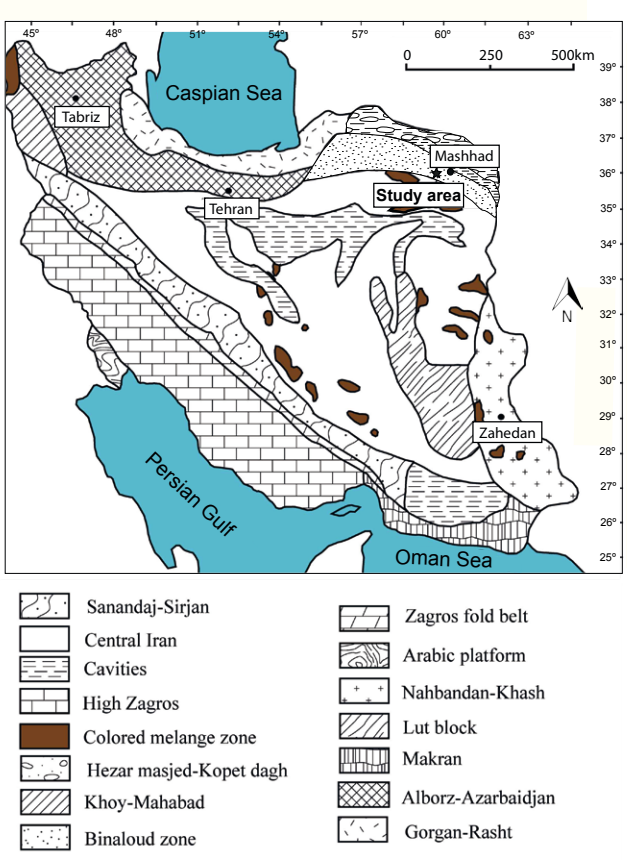

FIGURE 1. Simplified structural map of Iran and adjacent regions (after Nabavi, 1976).

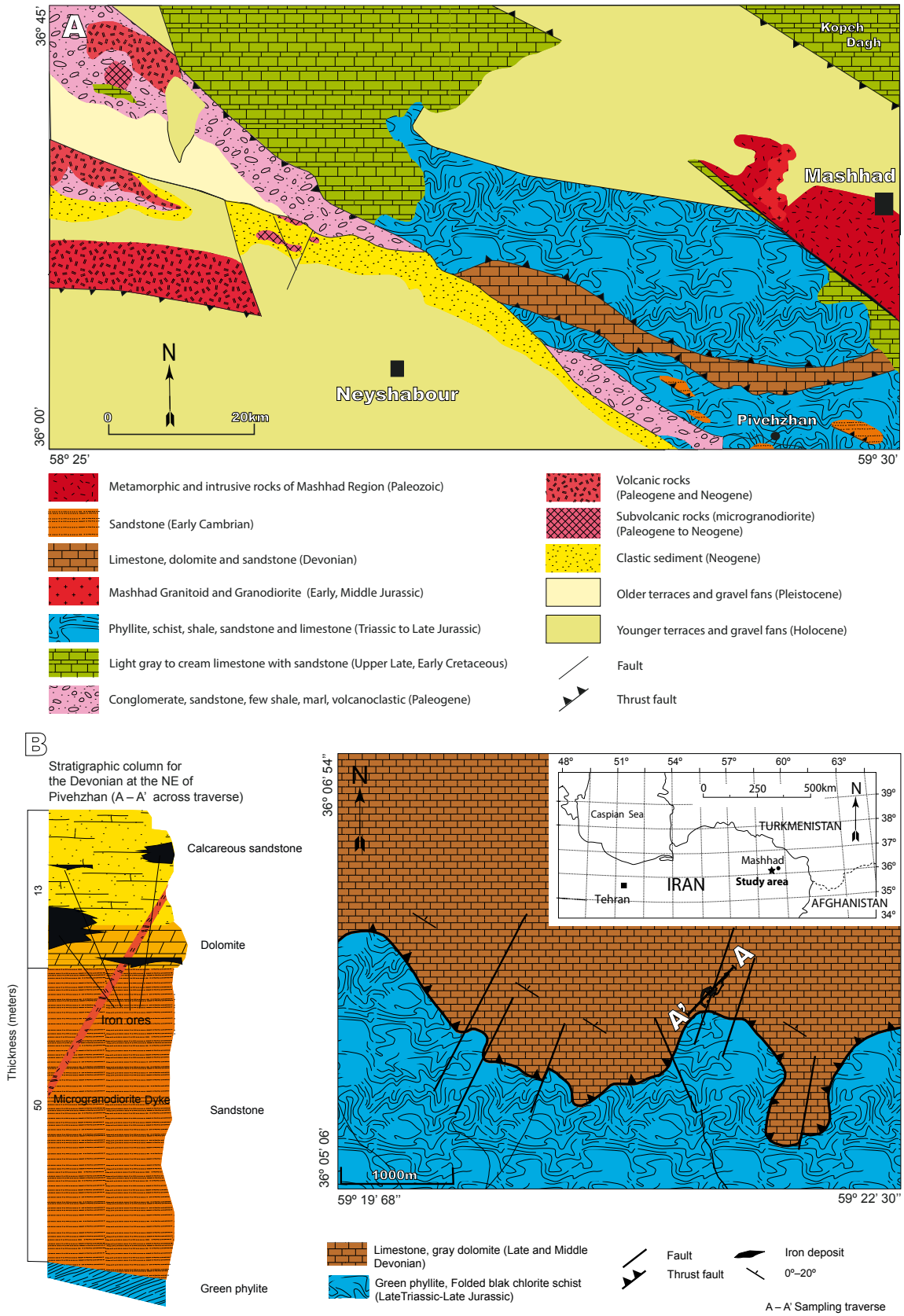

FIGURE 2. A) Geologic map of the Binaloud Zone modified after Lammerer *et al.* (1983). B) Geologic map and stratigraphic column of the Pivehzhan area in the Binaloud Zone, southwest of Mashhad, showing iron ores within dolomite and calcareous sandstones (see text for details).

According to Wendt *et al.*, (2005) the Paleozoic in the Iranian Region is characterized by shallow marine deposits. Paleozoic rocks consist of Early Cambrian sandstone and Silurian to Devonian carbonates. The lowermost Cambrian formation is characterized by well-defined sandstone beds (quartz-arenites, sub-litharenites, and Fe-bearing sandstones) and conglomerates. The slightly metamorphosed Silurian sandstones are usually characterized by the occurrence of well-developed ripple mark and desiccation cracks (Wauschkuhn *et al.*, 1984). The Middle-Upper Devonian formation consists of weakly metamorphosed limestone (Wendt *et al.*, 2005) and a relatively thick succession (310m) of carbonate rocks, which conformably overlies the older units (Wauschkuhn *et al.*, 1984). The lower part of the sedimentary sequence is dark gray in colour, indicating the presence of organic material. It is followed by calcareous sandstones, dolomites and iron mineralizations (Wauschkuhn *et al.*, 1984). The upper part of the sequence appears predominantly light gray and is dominated by carbonate rocks containing interbedded limestones, which gradually terminate to shales, sandstones and dolomites (Wauschkuhn *et al.*, 1984).

The Mesozoic sediments (Triassic to Upper Cretaceous) are metamorphosed and transformed to slate, phyllite and meta-conglomerate. The Cenozoic sequence consists of continental sediments accompanied by volcanic and volcanoclastic rocks and lies unconformably on the Mesozoic sequence that, in turn, is unconformably covered by Quaternary alluviums.

The igneous rocks in the Binaloud Zone include basalts (Silurian), ultramafic intrusive rocks (Permian), granitoid and granodiorite (Early to Middle Jurassic) and volcanic rocks (Cenozoic). Basic lava flows and volcanic sills of Devonian age appear as intercalations within the Silurian sandstone succession (Wauschkuhn *et al.*, 1984). They were formed in the west-northwest of Pivehzhan. The Permian ultramafic rocks intruded low- to medium-grade metamorphic sediments of probably oceanic origin (Lammerer *et al.*, 1983). They consist of basalts and picritic lavas (Holzer and Moemenzadeh, 1969; Davoudzadeh *et al.*, 1975). Granitoid and granodiorite (Early to Middle Jurassic) intruded the older Permo-Triassic rocks (Alavi, 1992). The Cenozoic igneous rocks consist of Eocene calc-alkaline andesite, Oligocene-Pliocene dacite, and Miocene-Pliocene high-K alkaline to shoshonitic basalt (Spies *et al.*, 1983).

The most important mineralizations present in the Binaloud Region include vein/veinlet of metallic elements like Au, Cu, Pb, and Zn hosted in volcanic rocks sometimes accompanied by non-metallic deposits of bentonite, halloysite, feldspars, and quartz (Ghorbani, 2013). Moreover, some supergene ironstones have occurred in the Cambrian sandstones (Najafzadeh Tehrani *et al.*, 2013) and some Fe, Pb, Zn and Ba mineralizations are found in the Devonian carbonates (Wauschkuhn *et al.*, 1984). Wauschkuhn *et al.* (1984 hypothesized that a possible source of Fe, Pb, Zn and Ba could be related to the submarine volcanism that intruded the Silurian sediments. Furthermore, Najafzadeh Tehrani *et al.* (2016b) and Zarei *et al.* (2016) reported some apatite-magnetite prospects within Oligo-Miocene sub-volcanic rocks in the region.

Geology of the study area

The lithologic units in the studied area include Devonian sediments and Upper Triassic-Lower Jurassic metamorphic rocks (Fig. 2B). The Devonian sedimentary sequence from bottom to consists of thick-bedded sandstones and calcareous rocks; these rocks locally appear to be thrust-faulted. The main tectonic features in the area are WNW-ESE striking faults and fold axes (Langheinrich and Lammerer, 1979). A conspicuous geologic characteristic of these rocks is the existence of many joint sets (Fig. 3A).

Thick-bedded sandstones (gray to cream) are composed of quartz, feldspar, opaque minerals and calcite cement. Dark gray dolomite unit (3–5m-thick) is underlying the calcareous sandstones. These rocks are cut by white calcite veinlets, up to several centimeters-thick (1mm–5cm), as well as by the iron orebodies. The uppermost part of the unit, is characterized by the occurrence of calcite and iron-rich veinlets (Fig 3B), while the lower part consists of well-bedded rocks, rarely cut by quartz and iron veins. The calcareous sandstone is thin- to thick-bedded and varies from gray to green. These rocks are characterized by the occurrence of well-developed karstic features (caves, sinkholes), laminated and weakly metamorphosed appearance, and the frequency of vein/veinlet infilled by iron oxide.

Magmatic rocks include aplitic granite which occurs as dykes (~2m-wide) cutting the host carbonates. These rocks are barren and display white to gray colours and fine-grained texture. The above rock units to the South of the study area are thrusted over Upper Triassic–Lower Jurassic metamorphic units, which mainly include meta-sandstone, slate, and phyllite, ranging in colour from light to dark green. They show characteristic slaty cleavage and have severely been suffered fracturing and strong brecciation close to the thrust surface.

Most of the iron ores occurred within the carbonates (dolomite and calcareous sandstone adjacent to the fault zone. These mineralized zones have a NW-SE strike and ~30°SW dip, about 1000m-length, 5–10m-width and form different separate ore bodies. The dominant

morphology is tabular or lenticular, irregular lenses (Fig. 4A), irregular masses, veins/veinlets (Fig. 4B; C), and layers. These stratabound lenticular deposits have about 100–500m-length and 5–15m-width and consist chiefly of haematite and goethite which are accompanied by subordinate amounts of magnetite and pyrite. The massive ores are irregular with variable dimensions and consist mainly of goethite (with colloform and botryoidal textures), haematite (with boxwork texture), and medium- to coarse-grained (2–5mm) calcite and dolomite crystals. The layered ores have 1–100cm-width and consist chiefly of Fe-oxides. The iron ores within veins/veinlets consist of magnetite, haematite, and goethite, accompanied by lesser amounts of Fe-sulphides and have variable thickness (10–200cm). In this type of ores, magnetite and Fe-sulphides occur as disseminated remnants, commonly found near the former open-spaces. The most important characters are corrosion and replacement of carbonate host by the iron oxides (Fig. 4D).

Petrography of country rocks and iron ores

The Devonian calcareous sandstone consists of monocrystalline quartz (~20%), albite (~20%), calcite (~40%), muscovite (10%) and iron-oxides (~3%), showing lepidoblastic and ultramylonitic textures. Calcite is mainly present as cement (Fig. 5A).

Dolomite rocks are composed of dolomicrosparite (15–60μm) and relatively coarser dolomite crystals (250–1000μm). These crystals are anhedral to subhedral with conspicuous cleavage (Fig. 5B). Quartz, muscovite, plagioclase, biotite, magnetite and pyrite, are disseminated in the dolomite and open spaces within it.

The aplitic dykes have granitic composition and comprise quartz, plagioclase (albite), orthoclase, and biotite. Plagioclase crystals are tabular, euhedral and relatively unaltered with normal zoning, poly-synthetic twinning and poikilitic texture.

Magnetite crystals are fine-grained (20–200μm), anhedral to euhedral (Fig. 5C). Haematite shows massive, boxwork and skeletal replacement textures. Goethite displays a typical colloform and botryoidal texture (Fig. 5D). Pyrite occurs as anhedral and dispersed crystal, filling the fractures. Two generations of pyrite (primary and secondary) were recognized in this deposit. The primary pyrite replaces magnetite (Fig. 5E) and was likely formed simultaneously with or shortly after it. The secondary pyrite occurs in veins and veinlets along with calcite, cutting the primary pyrite. Pyrrhotite occurs as fine-grained anhedral crystals engulfing islands of tiny magnetite crystals.

Hydrothermal alteration and mineralization

Based on field relations, petrographic investigations, and X-Ray Diffraction (XRD) analyses, two distinct alteration and mineralization stages were recognized at Pivehzhan as a result of hypogene and supergene processes (Fig. 6).

The hypogene alteration arose as replacement in dolomite and calcareous sandstone with formation of minerals such as calcite, sericite, chlorite, quartz, magnetite, pyrite, and pyrrhotite. This alteration halo is locally developed at Pivehzhan and is restricted to a narrow area about 50–100 meters around the mineralized zones. The fine sericite flakes were formed by alteration of detrital K-feldspars in the calcareous sandstone (Fig. 5F).

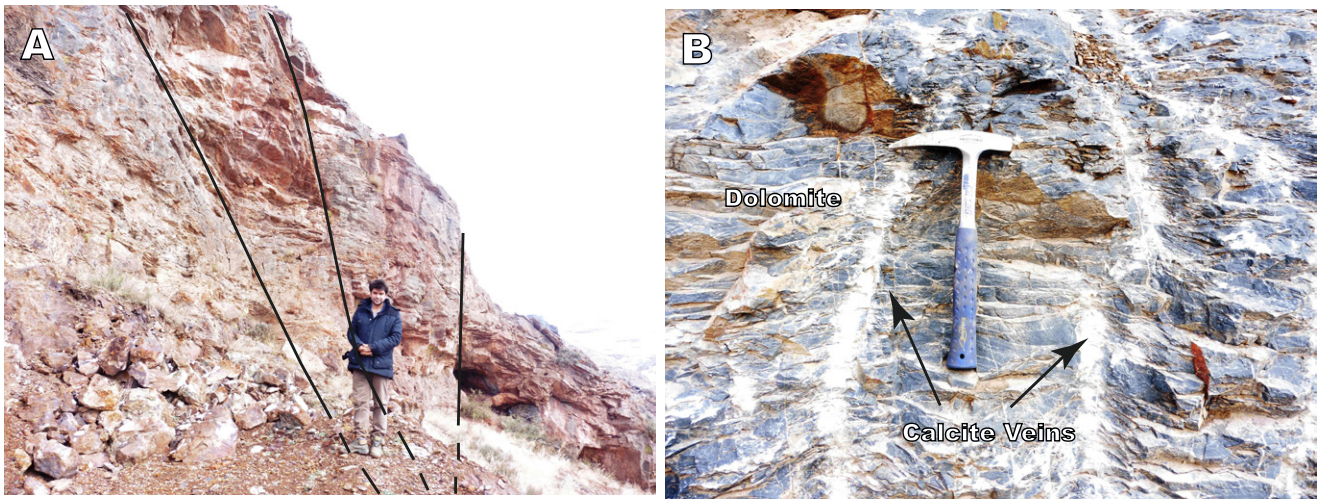

FIGURE 3. Field photographs of the host carbonates in the Pivehzhan area. A) Carbonate rocks with visible fractures and faults. B) Calcite veinlets within the dolomite.

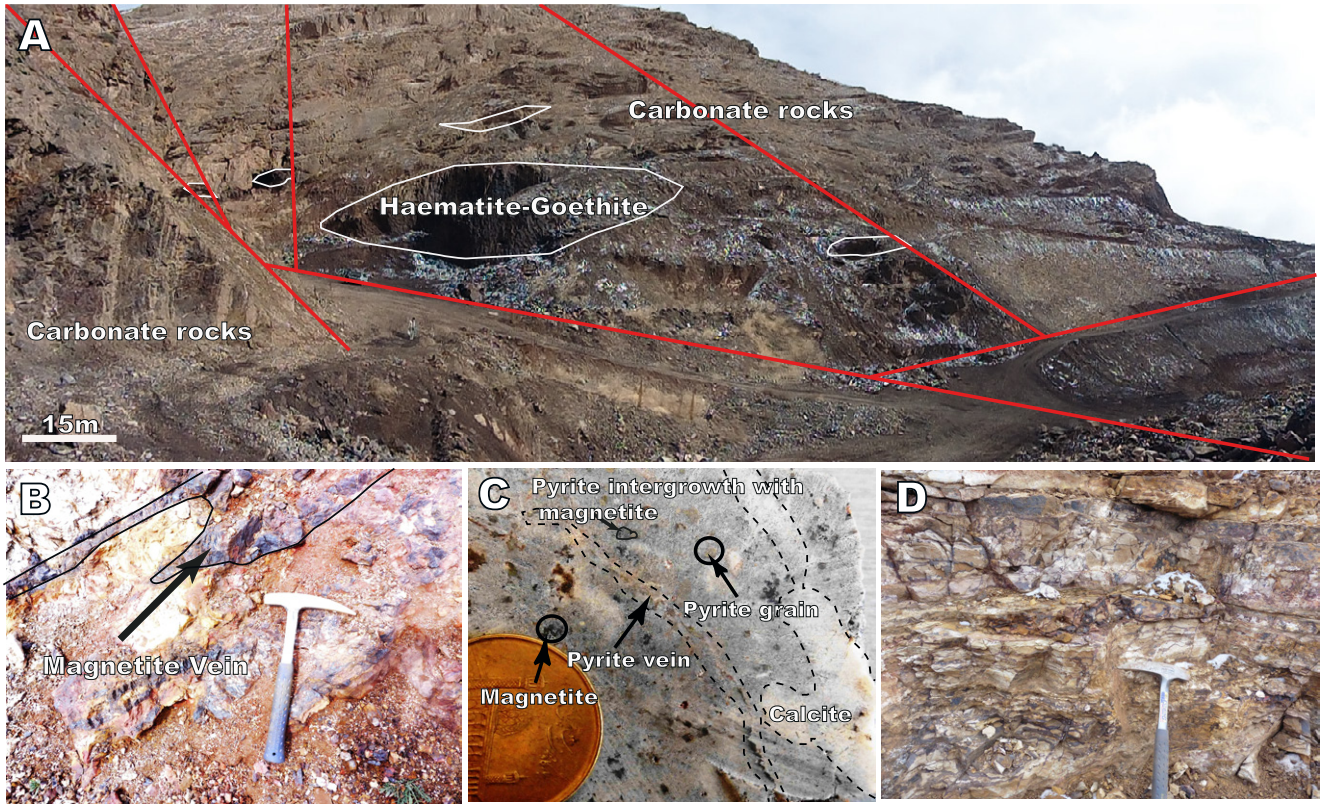

FIGURE 4. Field photographs of iron ores in the Pivehzhan area. A) Lens of iron ores (faults are in continues lines). B) Iron veinlets. C) Pyrite vein and granular pyrites showing intergrowth with magnetite. D) Carbonate host rock replaced by iron oxide.

The supergene alteration is characterized by the presence of minerals such as goethite, haematite, gypsum and halloysite in the carbonate rocks of this region. It is widespread and at the moment, mining operations are mainly focused on this zone.

The early hypogene stage responsible for the formation of euhedral magnetite crystals was likely occurred by the reaction of high-temperature acid solutions (<300°C; Barnes, 1997) with the enclosing carbonate rocks and the consequent increase in pH (Barnes, 1997).

METHODS OF INVESTIGATION

The study of the Pivehzhan iron deposit was performed in two stages, field and laboratory work. The field work included mapping and collecting systematic and random samples from the iron ores and host rocks along the selected traverses. The laboratory work began with preparation and petrographic examination of about 60 thin-polished sections. The samples with unclear mineralogy were analysed by XRD method. The chemical composition of the constituent minerals in the ores and host rocks were obtained by Electron Probe Micro-Analysis (EPMA) using wavelength dispersive spectrometry at the Mineralogy and Petrology Department of the Basque Country University (UPV/EHV), Spain, using a Camebax-Cameca equipped with 4 vertical spectrometers. Operating conditions for major elements in silicates included an accelerating voltage of 15kV, an electron beam current of 10nA and a beam diameter (source region) of 2μm. Counting times were 30s on the peak and 10s on each side of the background. For major elements, international standards from Spi Structure Probe Inc. were used and included: jadeite (Na-10.54wt.%), sanidine (K-10.05wt.%), diopside (Ca-18.39wt.%), spodumene (Al-14.50wt.%; Si-30.18wt.%), haematite (Fe-69.94wt.%), olivine (Mg-31.10wt.%), and pure metals (Mn and Ti). For trace elements analysis operating conditions were changed to 50nA and counting times of 90s. X-ray line interferences between elements were minimized and concentrations were corrected for major element matrix effects using the PAP matrix correction procedure (Pouchon and Pichoir, 1984). Detection limits were calculated with an accuracy of 2σ, at 95wt.% confidence level. The average detection limit for Ni, Co, Cu, Zn metals and As was around 500–300ppm.

Representative samples from the iron mineralization were selected for chemical characterization. All major (as wt.%) and trace elements (As, Ba, Co, Cu, Cr, F, Mo, Ni, Nb, Pb, Rb, S, Sr, V, W, Y, Zn, Zr,

Cs, Th, Sn; expressed as ppm) were determined by Wavelength Dispersive X-Ray Fluorescence (WDXRF) using a PANalytical Axios Advanced PW4400 XRF spectrometer (4kW Rh anode SST-mAX X-ray tube) at the Servicios Generales de Investigación (SGIker) of the Basque Country University. Fused beads were prepared by mixing 0.2g of finely ground sample with 3.8g of a lithium borate flux (Spectromelt A12, Merck) and LiBr as non-wetting agent. The lower detection limit for major elements and trace elements are about 0.01wt.% and ~5ppm, respectively.

Four samples from the host carbonate rocks were also chemically analysed using ICP-MS method in SGIker labs at the UPV/EHV. Three samples of the host carbonates and four of hydrothermal calcites coexisting with iron-oxides were analysed for C and O stable isotopes (using MAT-253 continuous spectrometer) in the laboratory of the

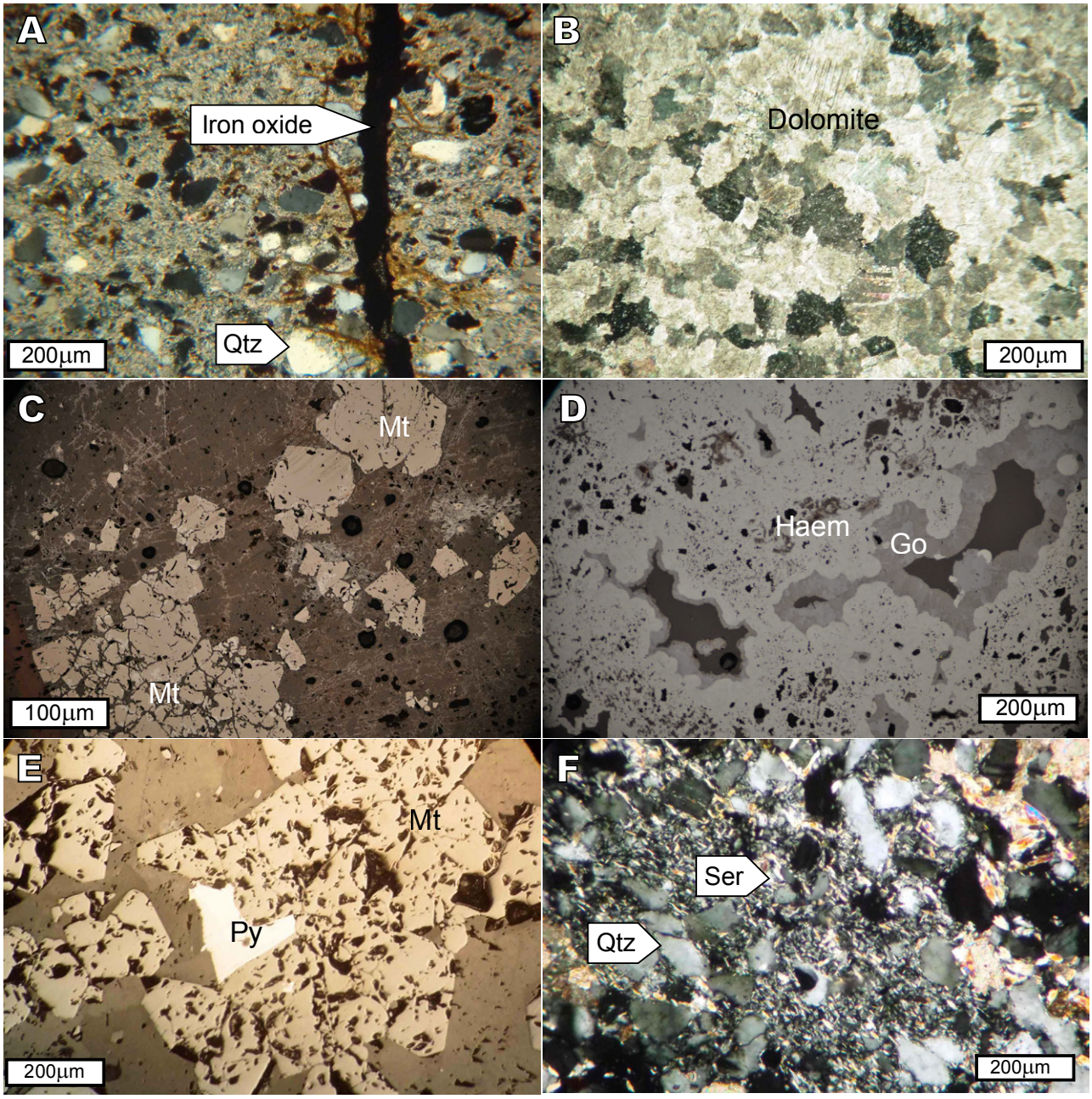

FIGURE 5. Photomicrographs of the host rocks and the iron ores at Pivehzhan. A) Host calcareous sandstone containing veinlets of Fe-oxides (xpl). B) Subhehral to euhedral recrystallized dolomite with sub-planar crystal boundaries (xpl). C) Euhedral magnetite crystals dispersed within the dolomite (xpl). D) Goethite with colloform texture (xpl). E) Intergrowth of Magnetite (Mt) and Pyrite (Py). F) Alteration of plagioclase to Sericite (Ser) in the calcareous sandstone (xpl). Abbreviation: Haem:Haematite, Mt:Magnetite, Go:Goethite, Py:Pyrite, Qtz:Quartz, Ser:Sericite.

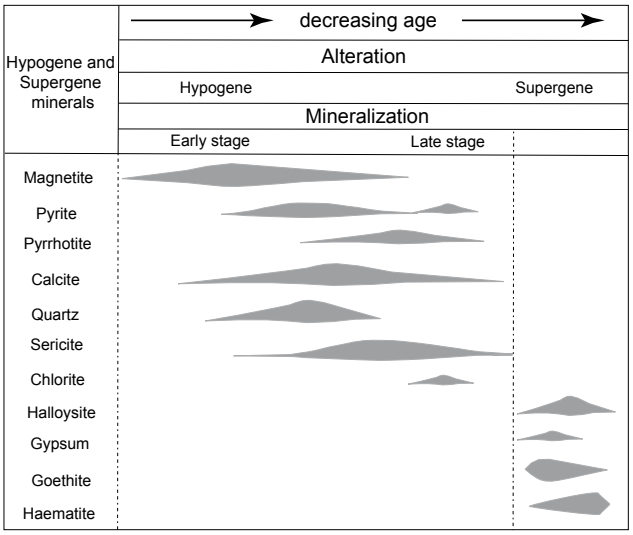

FIGURE 6. Paragenetic sequence of the constituent ore and gangue minerals in the Pivehzhan iron deposit.

Spanish National Research Council, in Madrid (Spain). Carbonate samples were converted into CO_2 by reaction with phosphoric acid at 100ºC, and the produced CO_2 was analysed in the mass spectrometer. All the analytical raw data were corrected using standard procedures (Craig, 1957) and reported in standard d-notation as per mil (‰) deviations relative to the Vienna-Standard Mean Ocean Water (V-SMOW) and PeeDee Belemnite (PDB) standards. Typical errors of reproducibility, 1σ, were ±0.1 for $\delta^{13}C_{PDB}$ and ±0.2% for $\delta^{18}O_{SMOW}$.

Fluid inclusion studies were mainly performed on doubly polished sections (~100μm-thick) of quartz (one sample) and calcite (four samples) veins/veinlets coexisting with magnetite and iron sulphides from the lower part of the deposit (unaltered zones). After microscopic examination, three sample wafers with measured isotopic composition were subjected to fluid inclusion analysis. They were analysed for salinity and Homogenization Temperature (T_H) using Linkam-THMS-600 stage equipped with heating (TP94) and freezing (LNP) controllers, attached to an Olympus petrographic microscope and a monitoring video apparatus in the Iranian Mineral Processing Research Centre, Karaj. The data were reproducible to ±0.2°C for freezing runs and ±6.0°C for heating runs. Stage calibration for heating mode was performed using cesium nitrate with the melting point of 414°C, for which the obtained precision was ±0.6°C. Stage calibration for freezing mode was carried out using n-hexane standard material with the melting point of -94.3°C, which yielded a precision of ±0.2°C.

Upon progressive heating, up to four phase transitions were observed in the inclusions, namely eutectic melting (T_e), ice melting ($T_{m(ice)}$) and Total Homogenization Temperatures ($T_{H(Total)}$). The bulk salinity of the fluid was calculated from $T_{m(ice)}$ (Steele-MacInnis *et al.*, 2011). Density calculations for the studied inclusions were carried out according to Bakker (2013) using the calculation method of Oakets *et al.* (1990).

RESULTS

The conditions of formation of the iron deposit were interpreted considering the changes experienced by the host rocks and ores, the chemistry of their minerals, composition and temperature of the fluids, isotopic changes in the host carbonates and the behaviour of rare earth and certain trace elements in the involved rocks.

Mineral chemistry of iron ores

According to data collected by Electron Probe Micro-Analyses (EMPA) we did not observe any major nor minor element variation (*i.e.* zoning) within single magnetite crystals (15 points). Major and trace element analyses of magnetite report mean values of V_2O_3~0.01wt.%, TiO_2~0.06wt.%, MnO~0.02wt.%, and MgO~0.01wt.% (Table 1), which are typical of hydrothermal deposits (Dare, *et al.*, 2014). This means that the concentration values of minor divalent (Mn^{2+}, Ni^{2+}, Mg^{2+}, and Zn^{2+}) and trivalent/tetravalent (Al^{3+}, V^{3+}, and Si^{4+}) cations within the magnetite crystal lattice are negligible. The analyses of pyrrhotite indicate a similar low amount of trace elements (minor amounts of As (~0.09wt.%), Co (0.01wt.%), and Ni (0.01wt.%) (Table 2)), according to which its composition is close to the stoichiometric formula of $Fe_{0.94}S$. Similarly, its compositional values do not show any variation from the centre of the crystal to its margins. Based on the average atomic composition (about 0.47atm% of Fe), it is suggested that monoclinic to intermediate hexagonal pyrrhotite in the Pivehzhan deposit were probably formed at temperatures below 300ºC, or even below 250ºC, according to Arnold (1969).

Bulk-rock geochemistry of the magnetite ores

The distribution of major oxides and trace elements across the iron deposit profile (Fig. 7) was studied on selected samples from: i) the lower horizon (Magnetite-rich, Mt, n=1), ii) intermediate horizon (Magnetite-Iron Sulphide-Iron Oxide, Mt-IS-IO, n=4) and iii) upper horizon (Haematite-Goethite-rich, Haem-Go, n=2). In general, except conspicuous variation in the concentration values of Si, Mn and As, the concentration of major oxides and rare elements in the three types of ores are similar (Fig. 8). The high Si concentration is due to the presence of silicate minerals and quartz coexisting with magnetite. The high Mn content in the haematite-goethite ores is due to the

adsorption of Mn^{2+} by Fe-oxides and/or -hydroxides in a supergene environment.

Results of the analyses (Table 3) show that the magnetite ores (i) have minor amounts of SiO_2 (~4.03wt.%), CaO (7.79wt.%), MnO (0.32wt.%) and Al_2O_3 (1.19wt.%); traces of Cr (71ppm), V (77ppm), Cu (413ppm), Pb (98ppm) and Zn (52ppm); and negligible amounts of Co and Ni.

Samples of magnetite-iron sulphide-haematite ores (ii) contain minor constituents like SiO_2 (~1.65wt.%), CaO (3.6wt.%), MnO (0.21wt.%) and Al (0.6wt.%), accompanied by trace amounts of Cr (69ppm), V (55ppm), Cu (544ppm), Pb (124ppm), Zn (93ppm) and As (199ppm). Finally, samples of haematite-goethite ores (iii), comprise minor amounts of SiO_2 (~1.15wt.%), CaO (14wt.%), MnO (4wt.%) and Al_2O_3 (0.7wt.%); traces of Cr (228ppm), V (50.44ppm), Cu (675.38ppm), Pb (87ppm) and Zn (116.2ppm); and negligible amounts of Co and Ni. Thus, these results imply that the intermediate horizon, formed by Magnetite-Iron Sulphide-Iron Oxide (Mt-IS-IO), is the richest in Fe and slightly rich in trace elements. The highest concentrations of As observed in samples from this horizon may easily be related to the presence of sulphides within these ores, while the overall high value reached by the CaO in these samples is due to the presence of hydrothermal calcite. Chromium concentration, that is usually used as discrimination index for iron deposits, reaches to values about 123ppm, which is far below the typically found range of Cr in iron ores of skarns and hydrothermal iron derived from Banded Iron Formations (BIF) (<458, <356ppm, respectively; according to Nadoll *et al.*, 2014). Conversely, Cr-values are similar to those found in some magmatic deposit (<10ppm; Nyström and Henriquez, 1994). The similarity of V^{3+} to Fe^{3+} in respect of size and change allows its substitution in the magnetite structure (Schuiling and Feenstra, 1980). Its concentration values (~57ppm) are far lower than typical magmatic ores (1000–2000ppm; Nyström and Henriquez, 1994) and thus, a magmatic origin seems unlikely for this element in Pivehzhan. Similarly, the mean TiO_2 concentration is about 0.05wt.% suggest a no-magmatic origin, which, in this case advocates a hydrothermal origin.

Fluid inclusion study

Five doubly-polished sections of calcite and quartz veins were examined under microscope in order to determine the distribution pattern, shape, size, phase content and paragenetic characteristics of the fluid inclusions. Most of the analysed fluid inclusions are irregular, elongate, polygonal, and rarely rhombic in shape. They include randomly distributed primary

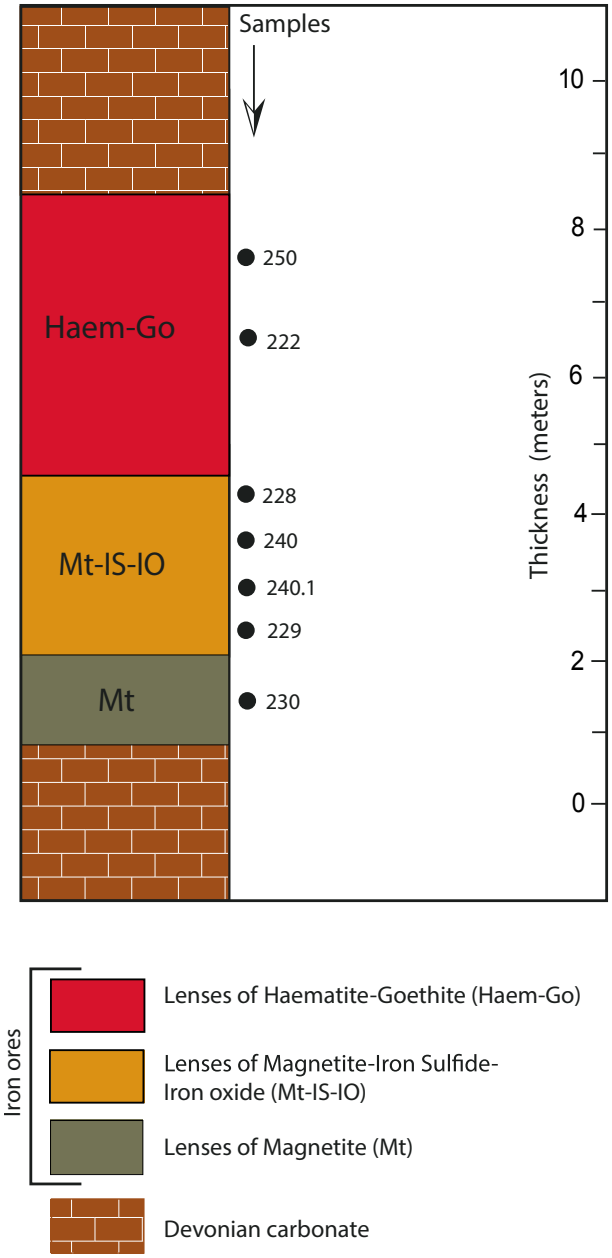

FIGURE 7. Stratigraphic column (across-traverse - Pivehzhan) of the studied iron deposit, showing the location of samples taken for geochemical analyses (black circles). See Figure 1 for the trend of sampling profile.

inclusions (7–30μm), as well as trails of secondary fluid inclusions (<5μm) (Fig. 9A; B). The majority of primary inclusions are present in two phases (liquid+vapor) at room temperature. Secondary inclusions are characterized by their distribution as trails cross-cutting the grain boundaries. Their estimated degree of fill (the volumetric proportion of liquid phase to total volume of the inclusion (Shepherd *et al.*, 1985)) is about 70–80%. Based on microthermometric measurements, the last $T_{m(ice)}$ and the estimated salinity range from -6°C to -0.7°C, and from 9.41wt.% to 0.4wt.% NaCl eq., respectively (Table 4).

TABLE 1. Electron Probe Micro-Analyses (EPMA) of magnetite crystals from the Pivehzhan iron ore samples

Sample	238	238	238	238	238	230	230	230	230	230	230	230	228	228	228
SiO_2	0.29	0.29	0.35	0.31	0.39	0.45	0.2	0.2	0.21	1.01	0.4	0.27	0.26	0.28	0.46
FeO	32.16	25.72	25.62	26.03	26.24	33.95	31.17	30.14	28.96	30.89	31.22	29.88	30.38	30.24	31.51
Fe_2O_3	70.96	69.98	69.72	70.81	71.38	64.24	67.25	68.01	68.4	66.65	67.35	67.42	68.55	68.23	67.99
Al_2O_3	0.13	0.13	0.18	0.15	0.16	0.3	0.13	0.18	0.13	0.32	0.12	0.17	0.19	0.18	0.2
MgO	0	0.01	0.02	0.01	0.02	n.d.	0.05	n.d.	0.04	n.d.	n.d.	n.d.	n.d.	n.d.	n.d.
TiO_2	0	0	0.05	0	0.08	0.16	0.09	0.1	0.03	0.07	0.07	0.1	0.06	0.06	0.01
MnO	0.04	0.02	0.01	0.01	n.d.	n.d.	0.07	n.d.	n.d.	n.d.	0.05	0.04	0.04	n.d.	n.d.
Cr_2O_3	0	0.02	0.01	n.d.	n.d.	0.03	n.d.	n.d.	0.05	n.d.	n.d.	n.d.	n.d.	n.d.	0.05
NiO	0.01	0.04	0.03	0.03	0.03	0.05	0.04	0.14	n.d.	n.d.	0.03	0.08	0	0.02	n.d.
V_2O_3	0.04	0.05	0.03	0.01	0.02	n.d.	n.d.	n.d.	0.01	n.d.	n.d.	0.01	0.03	0.03	n.d.
Formula pre-4-Oxygen (all Fe as FeO)															
Si	0.01	0.01	0.01	0.01	0.02	0.02	0.01	0.001	0.01	0.04	0.02	0.01	0.01	0.01	0.02
Fe''	1	0.85	0.85	0.85	0.85	1.11	1.01	0.98	0.95	0.99	1.01	0.98	0.98	0.98	1.01
Fe'''	1.98	2.08	2.07	2.08	2.07	1.88	1.97	1.98	2.01	1.93	1.96	1.98	1.99	1.99	1.96
Al	0.01	0.01	0.01	0.01	0.01	0.01	0.01	0.01	0.01	0.01	0.01	0.01	0.01	0.01	0.01

Abbreviations: n.d.: element not detected. Iron is reported as FeO and Fe_2O_3 according the redistribution of ΣFeO on the basis of charge balance and stoichiometry of magnetite.

However, most of the $T_{m(ice)}$ measurements show salinities ranging from 4.24wt.% to 5.30wt.%. NaCl eq.

During the heating process, most of the inclusions showed homogenization into liquid state by disappearance of vapor bubble, and their measured $T_{H(L-V)}$ values range from 129°C to 270°C. However, the maximum frequency distribution of T_H belongs to those with an average of 155°C (Table 4). The estimated densities for primary inclusions vary from 1.01g/cm^3 to 1.07g/cm^3 (Table 4) (Bakker, 2013).

Data points in the salinity *versus* $T_{H(L-V)}$ plot show a single population of fluid inclusions for which, T_H increases with the salinity decrease. This negative correlation (correlation coefficient of about 0.5) between salinity and T_H (Fig. 9C) suggests that the studied inclusions could have undergone natural stretching or leakage before the samples were collected (Fig. 9B).

C and O stable isotopes

Samples of dolomite (n=1), calcareous sandstone (n=2) and calcite veinlet (n=4) accompanying iron ores were selected for isotopic investigations. The calcite veinlets are intimately associated with pyrite, magnetite, haematite and goethite. The results of the isotopic analyses are listed in Table 5.

The carbon isotopic composition ($\delta^{13}C_{PDB}$) of the dolomite and calcareous sandstone (host carbonates) are -0.66‰, and -3.57‰ to -4.37‰, respectively. These results are lighter compared to those reported from Devonian marine carbonates, which range from 0.25‰ to 0.59‰ (Keith and Weber, 1964; Veizer and Hoefs, 1976).

Similarly, the carbon isotopic composition of the hydrothermal calcite (calcite veinlet) varies from -2.15‰ to -5.77‰ (with a mean of -4.24‰) which are analogous to the host carbonates. These slightly lighter carbon values of the calcite veinlet could be related to the interaction between hydrothermal fluids and the host carbonates during the mineralization processes.

The isotopic oxygen composition of the host dolomite and calcareous sandstone is about +19.20‰, and between +15.55‰ and +20.14‰, respectively (expressed as $\delta^{18}O_{SMOW}$), which are lighter than those of the Devonian carbonates (+23.33‰ to 23.68‰; Keith and Weber, 1964). The isotopic composition of oxygen ($\delta^{18}O_{SMOW}$) in hydrothermal calcite ranges from +19.87‰ to +21.64‰ (with a mean of +20.85‰) which is very similar to those supplied by the host carbonates.

Geochemistry of the host rocks

The total concentration values of REEs (ΣREE) in four representative samples of host rocks (three samples form the calcareous sandstone and one form the dolomite) range from 7.5ppm to 81.9ppm (analysed using Inductively Coupled Plasma-Mass Spectrometry (ICP-MS) method).

TABLE 2. Electron Probe Micro-Analyses (EPMA) of pyrrhotite crystals from the Pivehzhan iron ore samples

Sample	229	229	228	228	228	240	240	240	240	240	240	240
S	38.76	38.70	39.01	39.06	39.29	39.04	39.02	39.01	39.39	38.01	39.48	39.07
As	0.01	0.07	0.05	0.10	0.09	0.14	0.11	0.13	0.10	0.11	0.09	0.11
Sb	n.d.	n.d.	0.01	0.01	n.d.	0.03	n.d.	0.01	n.d.	n.d.	0.03	0.02
Fe	61.28	61.63	61.16	61.67	61.40	61.28	60.49	60.83	60.94	60.94	61.49	61.39
Cu	0.01	n.d.	0.10	0.05	n.d.	0.01	n.d.	0.02	n.d.	0.02	0.02	n.d.
Ni	n.d.	0.02	n.d.	0.03	0.02	0.01	0.02	0.03	0.01	0.02	0.03	0.01
Co	0.02	n.d.	n.d.	0.03	n.d.	n.d.	n.d.	0.04	n.d.	n.d.	0.03	n.d.
Mn	n.d.	0.02	n.d.	n.d.	n.d.	n.d.	0.01	n.d.	n.d.	n.d.	0.02	0.01
Cd	0.02	n.d.	0.03	n.d.	n.d.	n.d.	n.d.	n.d.	n.d.	n.d.	n.d.	0.02
Sn	0.09	0.02	n.d.	n.d.	n.d.	0.06	0.01	0.02	0.08	n.d.	n.d.	0.08
Zn	n.d.	0.04	0.01	n.d.	n.d.	n.d.	n.d.	n.d.	n.d.	0.01	n.d.	0.04
Hg	0.08	n.d.	n.d.	0.07	n.d.	n.d.	0.04	n.d.	0.01	0.03	n.d.	n.d.
Total	100.45	100.50	100.38	101.15	100.83	100.96	99.82	100.32	100.53	99.23	101.22	101.07
%atm Fe	0.48	0.48	0.47	0.47	0.47	0.47	0.47	0.47	0.47	0.48	0.47	0.47

Abbreviations: n.d.: element not detected.

While the highest-values are associated with the calcareous sandstone (containing calcite, quartz, and plagioclase), the lowest-values are associated with dolomite (see Table 6). The variation in the concentration of Light Rare Earth Elements (LREEs) is relatively large (between about 7 and 75ppm), whereas variation of Heavy Rare Earth Elements (HREEs) is slightly smaller (between 1 and 8ppm).

The distribution pattern of REEs normalized to Post-Archean average Australian Shale (PAAS; Fig. 10) shows that these elements suffered differentiation, the LREEs/HREEs ratio in the carbonates is in the range of 0.6–1.9.

La*/La anomalies, calculated following the of Bau and Dulski (1996) method with $La/La^*=[La/(3Pr-2Nd)]_{SN}$, indicate that in host carbonates have negative La anomalies (La/La*=1.12–6.75). The Y/Ho ratios in all samples range from 17.86 to 40.90. Eu and Ce anomalies are also important to understand the input effects of hydrothermal fluids.

To measure the anomaly values of Eu and Ce in the iron ores and the host rocks, the following equations were employed:

$$Eu/Eu^*=(Eu_N)/\sqrt{[(Sm_N)\times(Gd_N)]} \quad (1)$$

(Taylor and McLenan, 1985)

$$Ce/Ce^*=[Ce/(0.5La+0.5Pr)]_{SN} \quad (2)$$

(Bau and Dulski, 1996)

In the equation (2) SN stands for normalization of the elements to the composition of PAAS (McLennan, 1989).

The results indicate that Eu/Eu* ratios have a range of 0.84 to 3.88 in the calcareous sandstone and a value of 4.34 in the dolomite. Moreover, the Ce anomalies in the host carbonate rocks provided negative values (Ce/Ce*=0.78–0.96), which, although low, are significant.

DISCUSSION

There is little information on the Pivehzhan iron district to describe the main parameters, which have controlled the mineralization. The intense weathering affected the ores prevents a simple classification of these deposits, which include hydrothermal replacement, fillings and meteoric alteration superimposed on the almost completely disappeared primary mineralization. These issues are

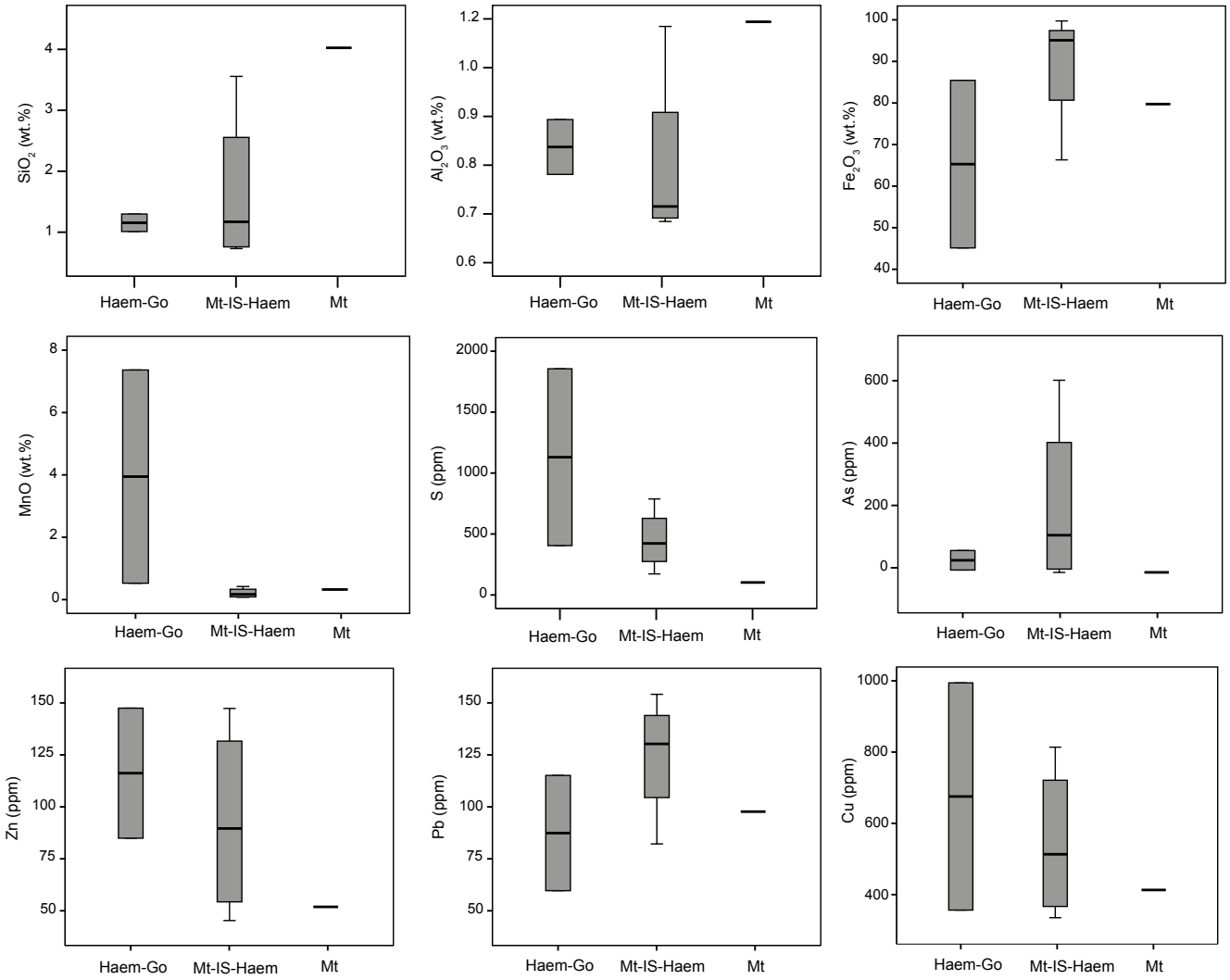

FIGURE 8. Concentration values of oxides (SiO_2, Al_2O_3, Fe_2O_3, MnO) and elements (S, As, Zn, Pb, Cu) in the Pivehzhan iron ores. Abbreviations: Haem:Haematite, Mt:Magnetite, Go:Goethite, IS:Iron Sulphide.

highly debatable and need clarification that can only be achieved by the combined geochemical study of the host rocks and the ores.

C and O isotope behaviour in host carbonate

The C and O isotopic values of carbonate-hosted Fe deposit plot very close to the field corresponding to the Phanerozoic and Devonian carbonates, as illustrated in Figure 11. According to this diagram, the C and O isotopic values of the Pivehzhan carbonates are lighter than those of Devonian carbonates.

Based on petrographical, mineralogical and geological data, it can be suggested that the $\delta^{13}C_{PDB}$ of the host carbonates suffered changes during hydrothermal alteration processes. The apparent variation in $\delta^{13}C_{PDB}$ in carbonate rocks occurs as the result of minor changes in pH and fO_2, variations in the rate of solubility, and/or dissolution of host carbonates in the course of low-temperature fluid circulation. The pH and fO_2 increase in the fluids (Ohmoto and Rye, 1979; Ohmoto, 1986) and/or dissolution of carbonates (Ohmoto, 1972) commonly lead to the increase of light carbon. It seems that the decarbonation of the marine limestone during hydrothermal metasomatism caused the $\delta^{13}C_{PDB}$ decrease in these rocks.

Moreover, if carbonate ions from the hydrothermal solutions were derived from dissolution of carbonate rocks at high-temperature, and reached isotopic equilibration, a large variation in initial $\delta^{18}O_{SMOW}$ toward lower-values would have occurred. Isotopic composition of host carbonates, along with their age, suggests that they have been suffering isotopic exchange reaction during thermal metamorphism. As a result of such an interaction, the

TABLE 3. Chemical analyses obtained by X-Ray Fluorescence (XRF) method for major and minor elements in samples of the Pivehzhan iron ores. Abbreviations: Haem:Haematite, Mt:Magnetite, Go:Goethite, IS:Iron Sulphide

Sample	250	222	228	240	240.1	229	230
Ore lens	Haem-Go	Haem-Go	Mt-IS-Haem	Mt-IS-Haem	Mt-IS-Haem	Mt-IS-Haem	Mt
SiO_2 (wt.%)	1.30	1.01	0.73	0.79	1.55	3.56	4.03
Al_2O_3	0.79	0.56	0.46	0.37	0.40	1.17	1.19
Fe_2O_3	85.44	45.13	99.73	95.04	95.12	66.32	79.73
MnO	7.36	0.53	0.08	0.24	0.10	0.42	0.32
MgO	0.01	0.25	b.d	n.d.	0.04	0.40	0.09
CaO	0.21	27.55	0.95	0.16	0.12	13.09	7.79
Na_2O	0.01	0.01	b.d	0.02	b.d	b.d	0.17
K_2O	0.08	0.03	n.d.	0.01	0.05	0.03	0.09
TiO_2	0.05	0.04	0.03	0.02	0.04	0.10	0.05
P_2O_5	0.01	0.04	0.01	0.02	0.03	0.02	0.02
As (ppm)	b.d	55.33	6.54	202.41	601.49	b.d	b.d
Ba	883.25	275.25	592.09	753.38	612.20	432.70	411.17
Co	b.d	4.21	b.d	b.d	23.92	19.38	b.d
Cu	994.20	356.56	813.84	335.23	628.11	398.41	413.03
Ni	70.12	94.73	b.d	b.d	b.d	25.64	b.d
Pb	115.12	59.66	133.78	126.78	154.14	82.17	97.70
S	1855.49	404.78	172.57	787.80	469.14	376.41	102.51
Zn	147.47	84.93	63.29	147.35	115.90	45.29	51.88
V	68.86	32.03	76.73	52.05	47.02	44.29	77.37
Cr	100.10	356.10	91.31	57.99	62.00	65.00	71.00

Abbreviations: b.d.: below detection

$\delta^{18}O_{SMOW}$ values of dolomite and calcareous sandstone have decreased to 4.48‰, 8.13‰ and 3.53‰, compared to the typical values of Devonian carbonate rocks (+23.33‰ to 23.68‰; Keith and Weber, 1964).

The origin of ore-forming fluids

The bivariate plot of $\delta^{18}O_{SMOW}$ *versus* $\delta^{13}C_{PDB}$ of the host carbonates and calcite veinlet (Fig. 11) illustrates that the isotopic values are close to those of the marine sediments. The relatively lower-values of $\delta^{13}C_{PDB}$ and $\delta^{18}O_{SMOW}$ of all samples is likely because of hydrothermal (metasomatic) and metamorphic processes affecting the initial isotopic composition of the original carbonate rocks.

REE behaviour in Carbonate host rocks

Studies carried out on REE patterns in post-Archean marine waters demonstrated that these waters were enriched in HREEs (Bau and Dulsky, 1996; Kamber and Webb, 2001; Shields and Webb, 2004). In the course of diagenesis, REEs content of carbonates remains almost constant (Banner *et al.*, 1988; Webb and Kamber, 2000; Nothdurf *et al.*, 2004). However, mixing of seawater with fluids of other sources (*e.g.* hydrothermal) brings about variation in their concentrations (Franchi *et al.*, 2015). This process in marbles affected by fluids of either metamorphic or magmatic or both origins caused depletion of LREEs as a result of adsorption and/or

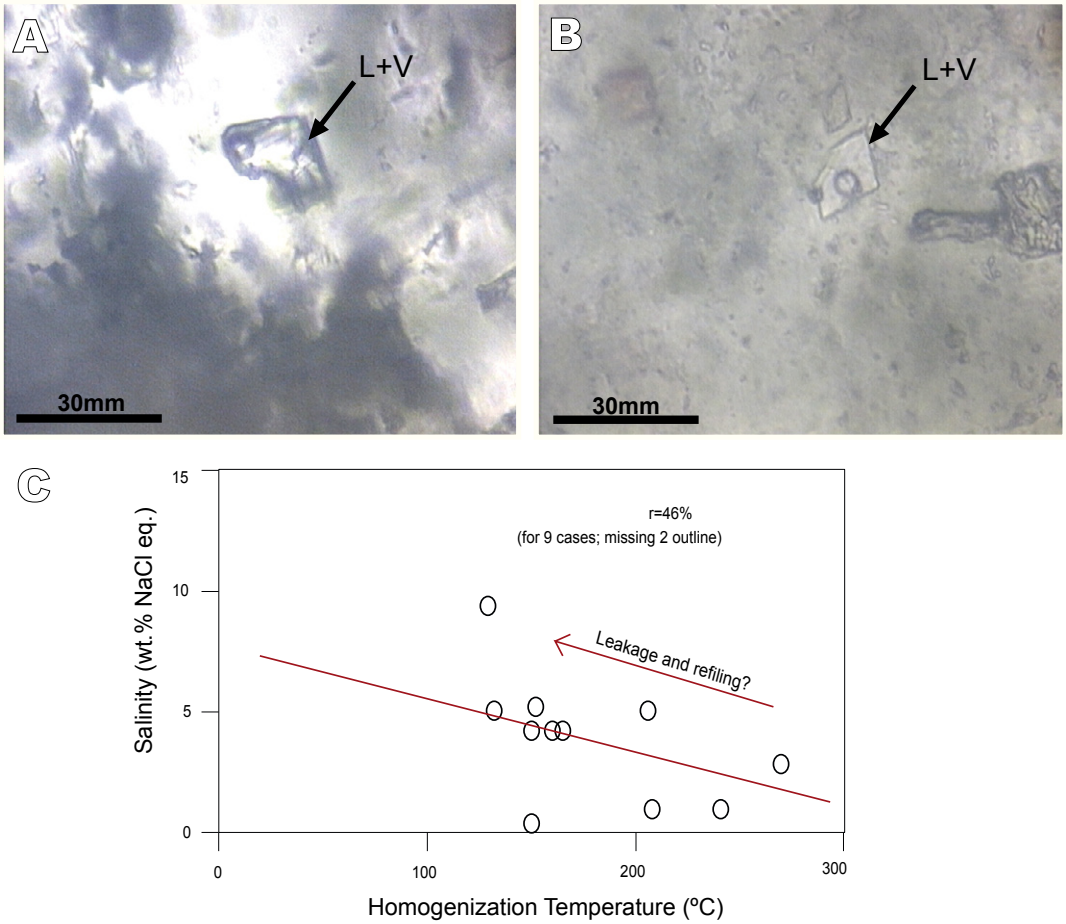

FIGURE 9. A) A polygonal liquid-rich 2-phase fluid inclusion in hydrothermal calcite crystals. B) A liquid-rich 2-phase fluid inclusion in hydrothermal quartz crystal, showing leakage. C) Bivariate plot of Homogenization Temperature (T_H) *versus* salinity, illustrating the data points of the liquid-rich 2-phase fluid inclusions in hydrothermal calcite and quartz crystals of the Pivehzhan iron ores.

transport by existing complexing (especially Cl^-) ligands (Rusinov *et al.*, 2008).

Nevertheless, considering the mineralogical composition of the studied carbonates and their positive Eu anomalies, it can be suggested that a notable proportion of LREEs were removed from the system during alteration of the host rocks. REEs are often transported by carbonate, sulphate, fluoride, and/or chloride complexes in hydrothermal solutions (Wood, 1990; Haas *et al.*, 1995; Migdisov *et al.*, 2016). Therefore, it seems that leaching and deposition of LREEs in the Pivehzhan carbonates is dependent not only on the marine origin of the sediments but also on the pH variation of altering solutions. Acidic pH is likely more suitable for leaching of LREEs during alteration of the host rocks. Considering the above-mentioned factors, the leaching of LREEs in the host rocks took place by infiltration of acidic hydrothermal solutions in the host rocks (Cantrell and Byrne, 1987).

The bivariate plots of $(LREEs)_{SN}$ and $(HREEs)_{SN}$ *versus* three major constituent oxides of the host rocks (*i.e.* Fe_2O_3, Al_2O_3, and SiO_2) (Fig. 12) demonstrate that Al-silicates played an important role in concentrating HREEs and, to a lesser extent, LREEs, whereas no such a role can be considered for Fe-bearing minerals in this regard.

Eu anomaly

The positive Eu anomaly customarily occurs as a result of the reaction of hydrothermal fluids with feldspars (McLennan, 1989). Nevertheless, it seems that the variation in the physico-chemical conditions of hydrothermal fluids in the course of migration plays an important role in developing such anomaly (Bau, 1991). If a hydrothermal fluid (with acidic characteristics) contains Eu^{2+}, this ion is less absorbed relative to trivalent REE cations, and thus may bring about positive Eu anomaly (Hecht *et al.*, 1999). Moreover, the low-fO_2 (below the magnetite/haematite buffer) and relative high-temperature (200–250ºC) of the fluid may contribute to the development of such an anomaly (Sverjensky, 1984;

TABLE 4. Summary of microthermometry data of fluid inclusions. All temperatures in °C. Salinity expressed as wt.% NaCl eq. X_{NaCl}: mole fraction of NaCl; $T_{m(ice)}$: final ice melting Temperature; T_H: Homogenization Temperature

Sample	Mineral	Inclusion types	Size (μm)	$T_{m(ice)}$ (°C)	$T_{H(L-V)}$	Mode	wt.% NaCl eq.	Density
1	Quartz	Primary L+V	10	-3.1	152	L+V=>L	5.23	1.04
2	Quartz	Primary L+V	15	-6	129	L+V=>L	9.41	1.07
3	Quartz	Primary L+V	12	-2.5	150	L+V=>L	4.24	1.03
4	Quartz	Primary L+V	17	-3	132	L+V=>L	5.07	1.04
5	Quartz	Primary L+V	5	-2.5	165	L+V=>L	4.24	1.03
6	Quartz	Primary L+V	7	-3	206	L+V=>L	5.07	1.04
7	Quartz	Primary L+V	10	-2.5	160	L+V=>L	4.24	1.03
8	Calcite	Primary L+V	7	-0.7	208	L+V=>L	0.99	1.01
9	Calcite	Primary L+V	5	-0.7	241	L+V=>L	0.99	1.01
10	Calcite	Primary L+V	5	-1.7	270	L+V=>L	2.86	1.02
11	Calcite	Primary L+V	30	-0.4	150	L+V=>L	0.4	1.01

Bau, 1991; Bau and Möller, 1992). The other reason for the positive Eu anomaly in the calcareous sandstone may be in connection with the presence of detrital plagioclase. The positive Eu anomaly in dolomite, however, can be owing to the substitution of Eu^{2+} for Ca^{2+} in carbonate minerals. In general, the positive Eu anomalies in dolomite and calcareous sandstone in the Pivehzhan area are associated with the main stage of hypogene sulphide (pyrite and pyrrhotite) and magnetite mineralization, which occurred at high-temperature and low-fO_2.

Variations in Ce anomaly and environmental conditions

Cerium anomaly values in carbonate rocks can be used for perception of paleo-redox conditions of formation environment (Liu *et al.*, 1988). Therefore, negative Ce anomalies in marine sediments (0.2–0.4) (Elderfield and Greaves, 1982; Piepgras and Jacobsen, 1992) indicate oxic conditions for seawaters, while positive Ce anomalies testify to anoxic conditions (Olivier and Boyet, 2006; Oliveri *et al.*, 2010; Hu *et al.*, 2014) or to the presence of Ce-bearing iron

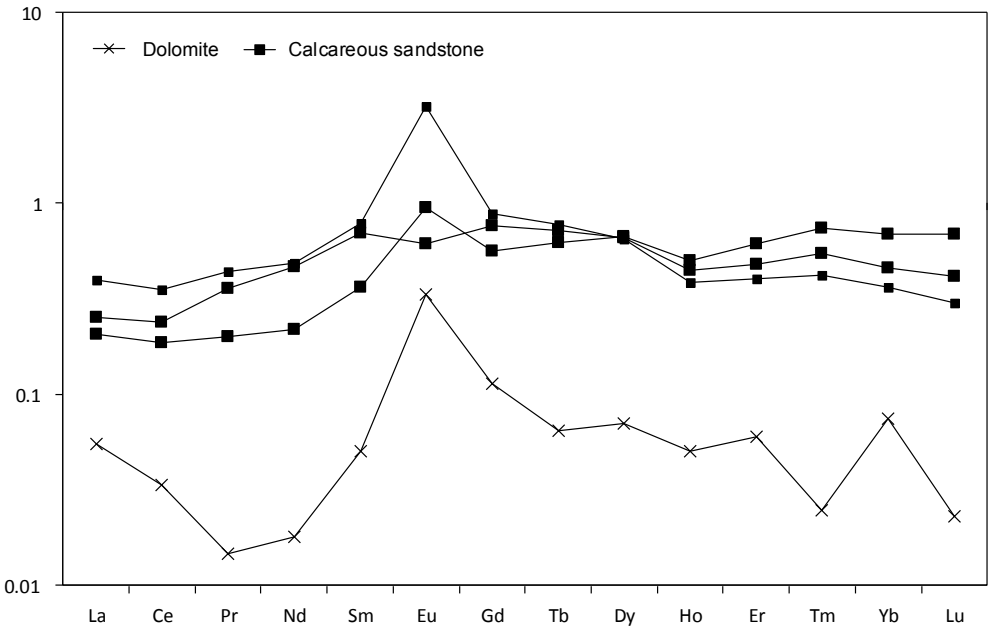

FIGURE 10. Distribution pattern of RareEarth Elements (REE) normalized to Post-Archean Australian Shale (PAAS) (McLennan, 1989) in the host carbonates in the Pivehzhan iron deposit.

TABLE 5. Carbon and oxygen isotopic data acquired from samples of host carbonates and hydrothermal calcite veinlets in the Pivehzhan iron deposit

Sample	Sample type	Associated mineral(s)	$\delta^{13}C$ (‰, VPDB)	$\delta^{18}O$ (‰, SMOW)
222	Hydrothermal calcite	Ca, Haem, Qtz	-3.40	19.87
230	Hydrothermal calcite	Ca, Go, Qtz	-2.15	21.64
242a	Hydrothermal calcite	Ca	-5.77	21.07
242b	Hydrothermal calcite	Ca	-5.67	20.88
252	Dolomite	Do, Ca	-0.66	19.20
224	Calcareous sandstone	Ca, Qtz , (+Mus)	-4.37	15.55
227	Calcareous sandstone	Ca, Qtz , (+Mus+Albite)	-3.57	20.14

Abbreviations: Ca: Calcite, Do: Dolomite, Go: Goethite, Haem: Haematite, Mus: Muscovite, Qtz: Quartz

hydroxides (Franchi *et al.*, 2015). The existence of detrital components (Nath *et al.*, 1997; Madhavaraju and Ramasamy, 1999; Madhavaraju and Lee, 2009; Madhavaraju *et al.*, 2010), diagenesis (Armstrong-Altrin *et al.*, 2003), scavenging processes (Bau *et al.*, 1996; Bau and Koschinsky, 2009), and paleo-redox conditions (Liu *et al.*, 1988) can also result in positive Ce anomalies in carbonate rocks.

The Ce anomaly values in the Pivehzhan carbonates are weakly negative (0.7–0.9), but are slightly greater than those of marine carbonates. The lack of correlation between Ce and certain oxides such as Fe_2O_3, Al_2O_3, and SiO_2 (Fig. 13A; B; C) may attest to the fact that detrital particles and iron oxides did not have any role in Ce concentration. Probably, the anoxic conditions created by hydrothermal fluids caused more Ce concentration in the host rocks relative to marine carbonates.

Y/Ho ratio

The Y/Ho ratio can furnish valuable information on seawater characteristics. Customarily, Y and Ho are regarded as geochemical twins (Bau, 1996) and hence they are expected to have similar geochemical behaviour in seawaters (Nozaki *et al.*, 1997). The Y/Ho ratio in clastic rocks and epiclastic sediments have a range of 26–28, while it shows a range of 44–74 in modern seawaters (Bau, 1996). Moreover, REEs of marine origin display a positive correlation between Y/Ho and La*/La ratios (Bau, 1996; Webb and Kamber, 2000; Allwood *et al.*, 2010).

The average value of Y/Ho ratio in the Pivehzhan carbonates is 34.78 and there is no correlation between Y/Ho and La*/La ratios (Fig. 13D), suggesting a detrital source for REEs.

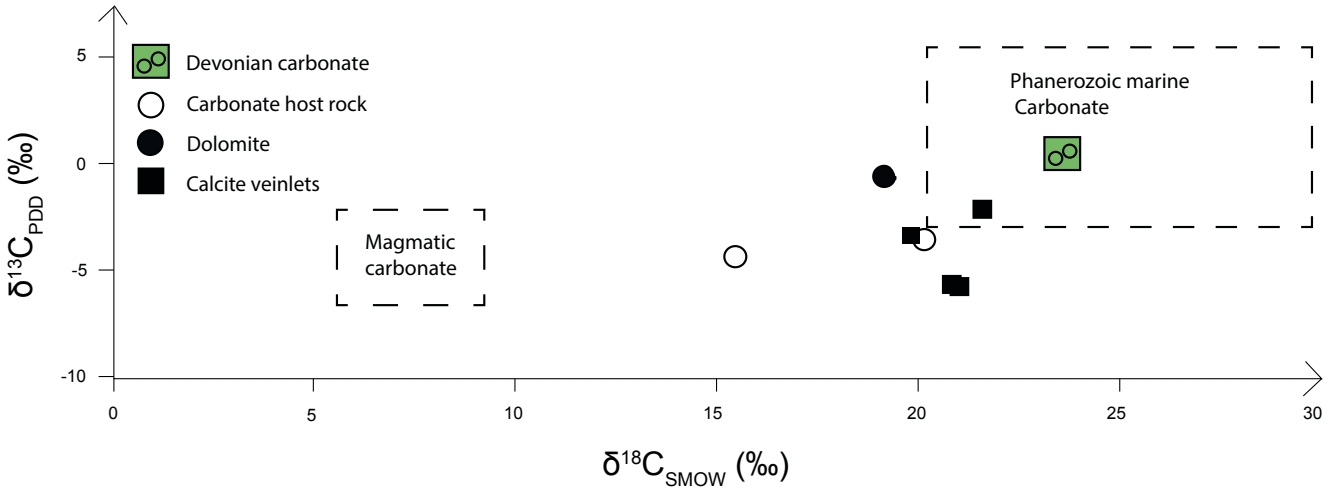

FIGURE 11. Bivariate plot of $\delta^{13}C_{PDB}$ *versus* $\delta^{18}O_{SMOW}$ of the carbonate rocks and calcite veinlet. The data points are clustered close to marine carbonates. Data of Phanerozoic marine carbonate from Veizer and Hoefs (1976), Devonian carbonate from Keith and Weber (1964) and magmatic carbonate from Taylor *et al.* (1967).

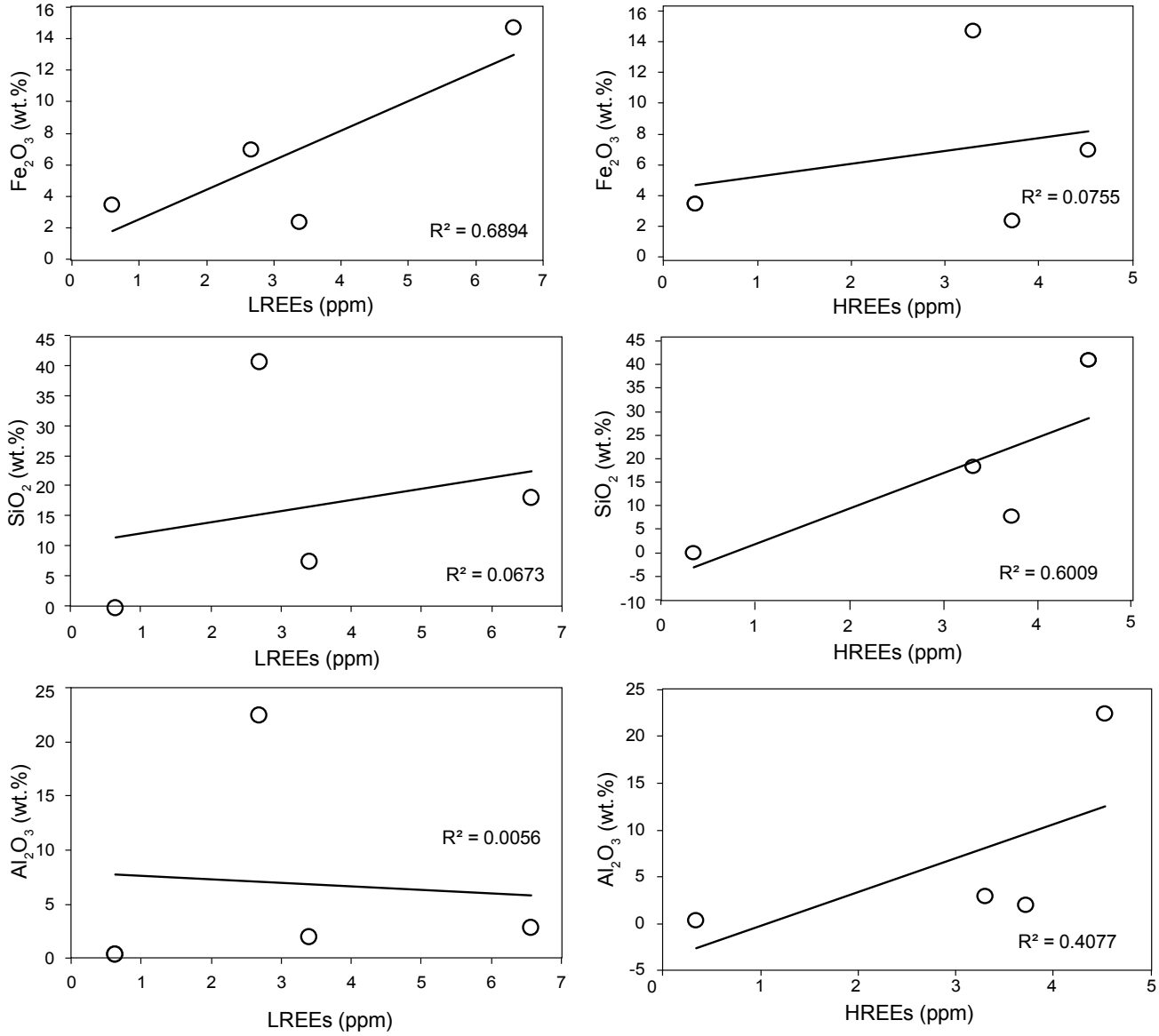

FIGURE 12. Correlations of Fe_2O_3, SiO_2, Al_2O_3 with LREEs and HREEs in the host carbonates of the Pivehzhan iron deposit. There is a positive correlation between LREE and Fe_2O_3, and between HREEs-SiO_2 and HREEs-Al_2O_3 pairs.

The iron ores' formation mechanism

Textural, mineralogical and geochemical data strongly suggest an epigenetic origin for the iron mineralization at Pivehzhan. The primary hydrothermal iron mineralization (comprised of magnetite, pyrite and pyrrhotite) was accompanied by recrystallization of the host dolomite and the formation of secondary products, such as calcite, quartz, sericite and chlorite during the hypogene alteration of the host rocks. Precipitation of magnetite in association with sulphides is the result of reaction between the host carbonate rocks with the Fe-rich hydrothermal solutions at low-fO_2 and -fS_2 conditions.

Since mineralization occurred as veinlet, stockwork, and open-space filling, in addition to carbonate-replacement iron ores, it can be deduced that secondary permeability and reaction with wall rocks were the most important factor for magnetite mineralization.

Simultaneous with magnetite formation, the reduction of sulphate to sulphide in the hydrothermal fluid was intensified (Barnes, 1997), giving rise to the formation of sulphides like pyrrhotite and/or pyrite.

Thus, by decreasing temperature, sulphides were formed and gradually replaced the primary magnetite (reaction 3):

$$Fe_3O_4+6H_2S+3O_2 => 3FeS+6H_2O \quad (3)$$

(Mitchell *et al.*, 1998)

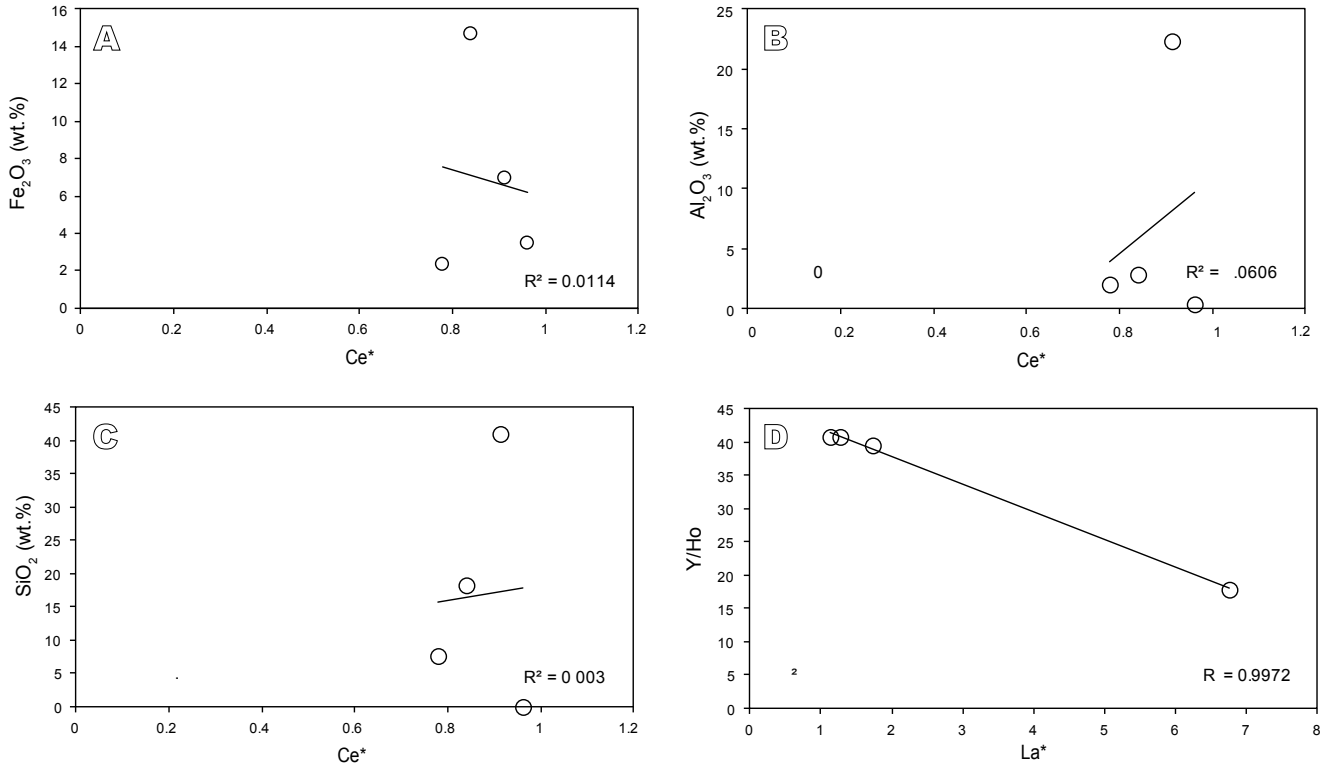

FIGURE 13. Correlations of A) Fe_2O_3, B) Al_2O_3, C) SiO_2 with Ce* and D) Y/Ho with La* in the host carbonates of the Pivehzhan iron deposit. There is no correlation between Ce* and the mentioned oxides and a negative correlation between Y/Ho and La*.

In fact, the presence of remnants of magnetite crystals within the sulphide minerals in the iron ores indicate that the formation of sulphides took place after the magnetite deposition.

The second generation of pyrite occurring as veinlets and open-space filling was precipitated during the late hypogene mineralization stage (Fig. 4C).

Since the mineralization occurred mainly at the margin of the fault zone, the ascending Fe-rich hydrothermal fluids brought about widespread iron mineralization along the brecciated zones. One reasonable source for iron might be the magmatic rocks existing at depth. It is likely that the hydrothermal solutions became enriched with iron by leaching these rocks and, upon ascending through the permeable zones of the reactive carbonate rocks, they precipitated the iron minerals (primary oxides and sulphides) (Hemley and Hunt, 1992).

Later, following the weathering and surficial erosion of the overburden rocks and falling of the paleo-water table, the hypogene mineralized zones were inundated by oxygenated descending waters. The hypogene magnetite and Fe-sulphides (pyrite and pyrrhotite) ores were almost completely oxidized to supergene Fe-oxides and -hydroxides along with sulphate. During these processes minerals such as goethite and haematite (limonite) were developed, preserving rare remnants of the primary mineral assemblages. Clear evidences of these type of transformations are found in the analysis of secondary textures (skeletal, botryoidal, pseudomorphs), which indicate the indigenous provenance of most of the iron ore concentrations.

The proposed model implies the flux of oxygenated descending water of meteoric origin, which reacts with the hypogene sulphides (magnetite and pyrite+pyrrhotite) and leads to the development of acid solutions, which are largely responsible of supergene alteration and mineralization. The existence of tremendous fault-induced cracks and fractures in the host rocks facilitated the circulation of the acid solutions to access to almost entire hypogene ore minerals. In the same way, the relatively higher primary porosity of the host calcareous sandstone, along with the secondary porosity (cracks and fractures) produced by faulting, brought about suitable conditions for pervasive supergene alteration of almost all the involved minerals.

TABLE 6. Results of the chemical analyses of major (wt.%), trace and Rare Earth Elements (REE) (ppm) on the altered host rocks of the Pivehzhan iron deposit

Sample	Calcareous sandstone 227	Calcareous sandstone 238	Calcareous sandstone 245	Dolomite 252
SiO_2 (wt.%)	7.72	18.32	40.95	n.d.
Al_2O_3	1.93	2.84	22.37	0.34
TiO_2	0.11	0.17	1.88	0.03
CaO	47.48	33.78	10.14	34.02
Fe_2O_3	2.35	14.67	6.94	3.43
K_2O	0.59	0.52	6.68	0.09
MgO	0.32	0.29	1.60	15.52
MnO	0.09	0.63	0.57	0.29
Na_2O	0.07	0.27	0.20	0.07
P_2O_5	0.04	0.05	0.21	n.d.
LOI	37.70	28.24	6.90	44.76
Ba (ppm)	56.89	45.57	1343.00	39.52
Co	7.54	5.18	11.51	0.40
Cr	14.58	17.08	609.00	4.02
Cs	0.31	0.73	6.17	0.35
Cu	102.20	69.22	52.85	70.81
Ga	3.11	4.77	34.00	0.60
Hf	0.85	3.82	2.82	0.32
Nb	6.36	8.70	13.21	1.53
Ni	13.12	15.51	59.19	n.d.
Pb	3.36	7.54	3.19	6.42
Rb	5.53	7.60	139.60	n.d.
Sc	2.42	1.19	36.20	n.d.
Sn	0.42	7.95	19.75	0.08
Sr	59.15	42.97	50.60	66.23
Ta	0.20	0.35	0.61	n.d.
Th	1.67	3.46	2.78	0.64
U	0.77	1.63	2.07	0.68

Abbreviations: n.d.: not detected, SN: normalization of elements to the composition of PAAS (McLennan, 1989).

TABLE 6. (Cont.)

Sample	Calcareous sandstone 227	Calcareous sandstone 238	Calcareous sandstone 245	Dolomite 252
V	14.52	21.47	248.00	0.41
Y	17.32	15.64	20.41	0.91
Zn	6.22	11.11	74.54	29.57
Zr	35.57	146.70	112.70	14.45
La	9.69	15.18	7.91	2.11
Ce	19.00	28.00	14.74	2.67
Pr	3.17	3.89	1.76	0.13
Nd	15.77	16.40	7.39	0.61
Sm	3.91	4.37	2.01	0.28
Eu	0.66	3.49	1.03	0.36
Gd	3.57	4.09	2.61	0.53
Tb	0.56	0.60	0.48	0.05
Dy	3.11	3.04	3.13	0.33
Ho	0.44	0.38	0.50	0.05
Er	1.37	1.14	1.74	0.17
Tm	0.22	0.17	0.30	0.01
Yb	1.30	1.03	1.95	0.21
Lu	0.18	0.13	0.30	n.d.
Eu/Eu*	0.86	3.89	2.11	4.34
Ce/Ce*	0.77	0.83	0.91	0.96
$LREE/HREE_{SN}$	0.91	1.98	0.6	1.77
Y/Ho	39.63	40.72	40.90	17.86
La/La*	1.75	1.12	1.27	6.83

Abbreviations: n.d.: not detected, SN: normalization of elements to the composition of PAAS (McLennan, 1989).

CONCLUSIONS

The isotopic investigations, petrographic examinations, and geochemical considerations in the Pivehzhan iron deposit demonstrated that mineralization of magnetite and Fe-sulphides in the host carbonates were resulted from the replacement of iron minerals by hydrothermal fluids. Based upon geochemical and microthemometric results, hot acidic (temperature ~200ºC), low-salinity (~5wt.%) and reducing hydrothermal fluids played an important role in the formation of the iron deposit. The distribution pattern of REEs and slightly negative Ce anomalies in host carbonates may reflect the affection of this rocks by the hydrothermal fluids, though their origin must not be neglected. Positive Eu anomalies and light carbon and oxygen isotopes in the carbonates represent a signature of hydrothermal fluids. The $\delta^{18}O_{SMOW}$ and $\delta^{13}C_{PDB}$ values of the host carbonates are slightly lower than those of marine

sediments, which may be due to the effect of metasomatic processes. The similarity of the isotopic composition of carbon and oxygen ($\delta^{13}C_{PDB}$ and $\delta^{18}O_{SMOW}$) of hydrothermal calcite with those of the host rocks suggests that CO_3^{2-} in the ore-forming fluids was derived from surrounding carbonate rocks. Geochemical data showed that the ores contain major oxides of Fe, S, Cu and Mn accompanied by insignificant amounts of Co, Ni, and V. The V and Ti contents of iron ore are lower than magmatic iron ores. Iron was likely sourced from leaching of subsurface magmatic rocks by hydrothermal fluids. Variation in the physico-chemical conditions of the hydrothermal solutions and their interaction with the host carbonates were the effective mechanism in the development of the iron ores at Pivehzhan. The absence of skarn minerals in the ores and/or in the margin of igneous rocks indicate that this deposit was developed merely by hydrothermal replacement with no involvement of skarnification processes and subjected to intense supergene leaching and enrichment at surface by meteoric solutions. The presence of boxwork, skeletal, colloform and botryoidal textures indicate strong replacement of sulphides by ironoxides and hydroxides in the supergene oxidized zone.

ACKNOWLEDGMENTS

Authors would like to express their thanks for financial and experimental support provided by the Research Deputy Bureau of the University of Tabriz (Iran), Basque Country University (Spain) and I. Mineral Processing Research Centre (Karaj). Also, authors would like to state their appreciation to Prof. Iñaki Yusta (Faculty of Science and Technology, Basque Country University) for letting us perform XRF analyses and to Dr. F. Tornos (Spanish National Research Council, Madrid) for facilitating the oxygen and carbon stable isotopic analyses.

Our gratitude is further extended to three anonymous reviewers, who have reviewed the manuscriptt and made critical comments and fruitful suggestions.

REFERENCES

Alavi, M., 1992. Thrust tectonics of the Binalood region, NE Iran. Tectonics, 11, 360-70.

Allwood, A.C., Kamber, B.S., Walter, M.R., Burch, I.W., Kanik, I., 2010. Trace elements record depositional history of an Early Archean strom a tolitic carbonate platform. Chemical Geology, 270, 148-163.

Armstrong-Altrin, J.S., Verma, S.P., Madhavaraju, J., Lee, Y.I., Ramasamy, S., 2003, Geochemistry of Late Miocene Kudankulam Limestones, South India. International Geology Review, 45, 16-26.

Arnold, R.G., 1969. Pyrrhotite Phase relations below 304+-6ºC at <11atm total pressure. Economic Geology, 64, 405-419.

Bakker, R.J., 2013. Software Package Fluids, version 2, Fluid inclusion laboratory Leoben. [Available at: http://fluids.unileoben.ac.at/Computer.html]

Banner, J.L., Hanson, G.N., Meyers, W.J., 1988. Rare earth element and Nd isotopic variations in regionally extensive dolomites from the Burlington-Keokuk Formation Mississippian: implications for REE mobility during carbonate diagenesis. Journal of Sediment and Petrology, 58, 415-432.

Barnes, H.L. (ed.), 1997. Geochemistry of hydrothermal ore deposit, 2nd edition. New York, John Wiley & Sons Inc., 972pp.

Bau, M., 1991. Rare-earth element mobility during hydrothermal and metamorphic fluid-rock interaction and the significance of the oxidation state of europium. Chemical Geology, 93, 219-230.

Bau, M., 1996. Controls on the fractionation of isovalent trace elements in magmatic and aqueous systems: evidence from Y/Ho, Zr/Hf, and lanthanide tetrad effect. Contribution. Mineralogy and Petrology, 123, 323-333.

Bau, M., Möller, P., 1992. Rare earth element fractionation in metamorphogenic hydrothermal calcite, magnesite and siderite. Mineralogy and Petrology, 45, 231-246.

Bau, M., Dulski, P., 1996. Distribution of yttrium and rare-earth elements in the Penge and Kuruman iron-formations, Transvaal Supergroup, South Africa. Precambrian Research, 79, 37-55.

Bau, M., Koschinsky, A., 2009. Oxidative scavenging of cerium on hydrous Fe oxide: evidence from the distribution of rare earth elements and yttrium between Fe oxides and Mn oxides in hydrogenetic ferromanganese crusts. Geochemical Journal, 43, 37-47.

Bau, M., Koschinsky, A., Dulski, P., Hein, J.R., 1996. Comparison of the partitioning behaviours of yittrium, rare earth elements, and titanium between hydrogenetic marine ferromanganese crusts and seawater. Geochimica et Cosmochimica Acta, 60, 1709-1725.

Bertram, C., Elderfield, H., 1993. The geochemical balance of the rare earth elements and neodymium isotopes in the oceans. Geochimica et Cosmochimica Acta, 57, 1957-1986.

Cantrell, K.J., Byrne, R.H., 1987. Rare earth element complexation by carbonate and oxalate ions. Geochimica et Cosmochimcal Acta, 51, 597-60.

Chen, D., Qing, H., Yan, X., Li, H., 2006. Hydrothermal venting and basin evolution Devonian, South China: Constraints from rare earth element geochemistry of chert. Sedimentary Geology, 183, 203-216.

Craig, H., 1957. Isotopic standards and isotopic correction factors for mass spectrometric analysis of carbon dioxide. Geochimica Cosmochimica Acta, 12, 133-149.

Dare, A.-S., Barnes, S.-J., Beaudoin, G., Méric, J., Boutroy, E., Potvin-Doucet, C., 2014. Trace elements in magnetite as petrogenetic indicators. Mineralium Deposita, 49, 785-796.

Davoudzadeh, M., Aghanabati, M., Shahrabi, M., 1975. An orogenic phase of mid-Jurassic age in northeast Iran Binalood Mountain rang. Neues Jahrbuch für Geologie und Mineralogie Abhandlungen, 162, 137-163.

Elderfield, H., Greaves, M.J., 1982. The rare earth elements in seawater, Nature, 296, 214-219.

Feng, D., Chen, D., Peckmann, J., 2009. Rare earth elements in seep carbonates as tracers of variable redox conditions at ancient hydrocarbon seeps. Terra Nova, 21, 49-56.

Fernández-Nieto, C., Torres-Ruiz, J., Pérez, I.S., González, I.F., López, J.G., 2003. Genesis of Mg-Fe carbonates from the Sierra Menera magnesite-siderite deposits, Northeast Spain: Evidence from Fluid inclusions, Trace elements, rare earth elements, and stable isotope data. Economic Geology, 98, 1413-1426.

Franchi, F., Hofmann, A., Cavalazzi, B., Wilson, A., Barbieri, R., 2015. Differentiating marine vs hydrothermal processes in Devonian carbonate mounds using rare earth elements Kess Kess mounds, Anti-Atlas, Morocco. Chemical Geology, 409, 69-86.

Ghorbani, M., 2013. The economic geology of Iran: mineral deposits and natural resources. New York, Springer Dordrecht Heidelberg, 581pp.

Greaves, M., Elderfield, H., Sholkovitz, E., 1999. Aeolian sources of rare earth elements to the Western Pacific Ocean. Marine Chemistry, 68, 31-38.

Haas, J.R., Shock, E.L., Sassani, D.C., 1995. Rare earth elements in hydrothermal systems: estimates of standard partial modal thermodynamic properties of aqueous complexes of the rare earth elements at high pressures and temperatures. Geochimica et Cosmochimica Acta, 59, 4329-4350.

Hecht, L., Freiberger, R., Gilg, H.A., Grundmann, G., Kostitsyn, Y.A., 1999. Rare earth element and isotope C, O, Sr characteristics of hydrothermal carbonates: genetic implications for dolomite-hosted talc mineralization at Göpfersgrün Fichtelgebirge, Germany. Chemical Geology, 155, 115-130.

Hemley, J., Hunt, J., 1992. Hydrothermal ore-forming processes in the light of studies in rock-buffered systems II, Some general geologic applications. Economic Geology, 87, 23-43.

Holzer, H.F., Moemen Zadeh, H., 1969. Report on reconnaissance of granite margins in the Mashhad area, Khorasan province, northeastern Iran. Tehran, Geological survey of Iran, 41pp. [Internal Report]

Hu, Y., Feng, D., Peckmann, J., Roberts, H.H., Chen, D., 2014. New insights into cerium anomalies and mechanisms of trace metal enrichment in authigenic carbonate from hydrocarbon seeps. Chemical Geology, 381, 55-66.

Jiang, S.Y., Zhao, H.X., Chen, Y.Q., Yang, T., Yang, J.H., Ling, H.F., 2007. Trace and rare earth element geochemistry of phosphate nodules from the lower Cambrian black shale sequence in the Mufu Mountain of Nanjing, Jiangsu province, China. Chemical Geology, 244, 584-604.

Kamber, B.S., Webb, G.E., 2001. The geochemistry of Late Archaean microbial carbonate: implications for ocean chemistry and continental erosion history. Geochimica et Cosmochimica Acta, 65, 2509-2525.

Kamber, B.S., Bolhar, R., Webb, G.E., 2004. Geochemistry of late Archaean stromatolites from Zimbabwe: evidence for microbial life in restricted epicontinental seas. Precambrian Research, 132, 379-399.

Keith, M., Weber, J.N., 1964. Carbon and oxygen isotopic composition of selected limestones and fossils. Geochimica et Cosmochimica Acta, 28, 1787-1816.

Kim, J.H., Torres, M.E., Haley, B.A., Kastner, M., Pohlman, J.W., Riedel, M., Lee, Y.-J., 2012. The effect of diagenesis and fluid migration on rare earth element distribution in pore fluids of the northern Cascadia accretionary margin. Chemical Geology, 291, 152-165.

Lammerer, B., Langheinrich, G., Manutchehr Danai, M., 1983. The tectonic evolution of the Binaloud NE-Iran, Geodynamic project Geotraverse in Iran, in geodynamic project in Iran, Geological Survey of Iran, Tehran, 51, 91-102. [Final report]

Langheinrich, G., Lammerer, B., 1979. Structural section through the Binaloud –Mountains- a preliminary report. Arbeitsbericht zum Forschungsvorhaben La, 212, 4, 17pp.

Liu, Y.G., Miah, M.R.U., Schmitt, R.A., 1988. Cerium: a chemical tracer for paleo-oceanic redox conditions. Geochimica et Cosmochimica Acta, 52, 1361-1371.

Madhavaraju, J., Ramasamy, S., 1999. Rare earth elements in limestones of Kallankurichchi Formation of Ariyalur Group, Tiruchirapalli Cretaceous, Tamil Nadu. Journal of the Geological Society of India, 54, 291-301.

Madhavaraju, J., Lee, Y.I., 2009. Geochemistry of the Dalmiapuram Formation of the Uttatur Group Early Cretaceous, Cauvery basin, southeastern India: Implications on provenance and paleo-redox conditions. Revista Mexicana de Ciencias Geológicas, 26, 380-394.

Madhavaraju, J., González-León, C.M., Lee, Y.I., Armstrong-Altrin, J.S., Reyes-Campero, L.M., 2010. Geochemistry of the Mural Formation Aptian-Albian of the Bisbee Group, Northern Sonora, Mexico. Cretaceous Research, 31, 400-414.

McLennan, S.M., 1989. Rare earth elements in sedimentary rocks influence of provenance and sedimentary processes. Reviews in Mineralogy and Geochemistry, 21, 169-200.

Migdisov, A., Williams-Jones, A., Brugger, J., Caporuscio, F., 2016. Hydrothermal transport, deposition, and fractionation of the REE: Experimental data and thermodynamic calculations. Chemical Geology, 439, 13-42.

Mitchell, P.A., Proffett, J.M., Dilles, J.H., 1998. Geological review of the Batu Hijau porphyry copper-gold deposit, Sumbawa Island, Indonesia. Newmont Nusa Tenggara Company, 164pp. [Final report] [Unpublished]

Nabavi, M., 1976. An introduction to the geology of Iran. Tehran, Geological survey of Iran, 109pp. [In Persian]

Nadoll, P., Angerer, T., Mauk, J.L., French, D., Walshe, J., 2014. The chemistry of hydrothermal magnetite: a review. Ore Geology Reviews, 61, 1-32.

Najafzadeh Tehrani, P., Calagari, A., Abedini, A., Mazlumi, A., 2013. Geological, mineralogical, alteration features, rare earth elemnts REE geochemistry of Neyzar Iron deposit, Southwest of Mashhad, Northeast Iran. Iranian Society of Crystallography and Mineralogy, 21, 229-242. [In Persian with English abstract]

Najafzadeh Tehrani, P., Calagari, A.A., Velasco Roldan, F., Simmonds, V., Siahcheshm, K., 2016a. Mineralogy and mineral chemistry of Pivehzhan iron deposit in northeast of Iran. 34th National and 2nd Internatinal Geoscience Congress of Geological Survey of Iran, Tehran. [In Persian with English abstract]

Najafzadeh Tehrani, P., Calagari, A.A., Velasco, F., Simmonds, V., Siahcheshm, K., 2016b. Mineral chemistry and geothermometry of Fe-Ti oxides in the Khanlogh magnetite-apatite ore, northwest of Neyshabour, NE Iran. Neues Journal für Geologie und Paläontologie-Abhandlungen, 281, 227-246.

Nath, B.N., Bau, M., Ramalingeswara Rao, B., Rao, Ch.M., 1997. Trace and rare earth elemental variation in Arabian Sea sediments through a transect across the oxygen minimum zone. Geochimica et Cosmochimica Acta, 61, 2375-2388.

Nothdurft, L.D., Webb, G.E., Kamber, B.S., 2004. Rare earth element geochemistry of Late Devonian reefal carbonates, Canning Basin, western Australia: confirmation of a seawater REE proxy in ancient limestones. Geochimica et Cosmochimica Acta, 68, 263-283.

Nozaki, Y., Zhang, J., Amakawa, H., 1997. The fractionation between Y and Ho in the marine environment. Earth and Planetary Science Letters, 148, 329-340.

Nyström, J.O., Henriquez, F., 1994, Magmatic Features of Iron Ores of the Kiruna Type in Chile and Sweden: Ore Textures and Magnetite Geochemistry. Economic Geology, 89, 820-839.

Oakas, C.S., Bondar, R.J., Simonson, J.M., 1990. The NaCl-$CaCl_2$-H_2O: 1. The ice liquid at 1 atom pressutre. Geochimica et Cosmochimica Acta, 54, 603-610.

Ohmoto, H., 1972. Systematics of sulfur and carbon isotopes in hydrothermal ore deposits. Economic Geology, 67, 551-579.

Ohmoto, H., 1986. Stable isotope geochemistry of ore deposits. Reviews in Mineralogy and Geochemistry, 16, 491-559.

Ohmoto, H., Rye, R.O., 1979. Isotopes of sulfur and carbon. In: Barnes, H.L. (ed.). Geochemistry of Hydrothermal Ore Deposits, New York, Wiley, 509-567.

Olivier, N., Boyet, M., 2006. Rare earth and trace elements of microbialites in Upper Jurassic coral- and sponge-microbialite reefs. Chemical Geology, 230, 105-123.

Oliveri, E., Neri, R., Bellanca, A., Riding, R., 2010. Carbonate stromatolites from a Messinian hypersaline setting in the Caltanissetta Basin, Sicily: petrographic evidence of microbial activity and related stable isotope and rare earth element signatures. Sedimentology, 57, 142-161.

Piepgras, D.J., Jacobsen, S.B., 1992. The behaviour of rare earth elements in seawater: precise determination of variations in the North Pacific water column. Geochimica et Cosmochimica Acta, 56, 1851-1862.

Pouchon, J.L., Pichoir, J., 1984. A new model for quantitative xray microanalysis. Part I: application to the analysis of homogeneous samples. La Recherche Aerospatiale, 3, 167-192.

Rusinov, V.L., Rusinova, O.V., Kryazhev, S.G., Shchegol'Kov, Y.V., Alysheva, E.I., Borisovsky, S.E., 2008. Wall- Rock metasomatism of carbonaceous Terrigenous rocks in the Lena Gold district. Geology of Ore Deposits, 50, 1-40.

Schuiling, R., Feenstra, A.A., 1980. Geochemical behaviour of vanadium in iron-titanium oxides. Chemical Geology, 30, 143-150.

Shepherd, T.J., Rankin, A.H., Alderton, D.H.M., 1985. A Practical Guide to Fluid Inclusion Studies. New York, Blackie, 239pp.

Shields, G., Webb, G., 2004. Has the REE composition of seawater changed over geological time? Chemical Geology, 204, 103-107.

Spies, O., Lensch, G., Mihem. A., 1983. Chemistry of post-ophiolithic tertiary volcanic between Sabzevar and Quchan, NE Iran. In: Almassi. A. (ed.). Geodynamic project geotravers in Iran, Geological survey of Iran, Tehran, 51, 247-266.

Steele-MacInnis, M., Bodnar, R.J., Naden, J., 2011. Numerical model to determine the composition of H_2O-NaCl-$CaCl_2$ fluid inclusions based on microthermometric and microanalytical data. Geochimica et Cosmochimica Acta, 75, 21-40.

Sverjensky, D.A., 1984. Europium redox equilibria in aqueous solution. Earth Planetary Science Letters, 67, 70-78.

Taofa, Z., Mingan, W., Yu, F., Chao, D., Feng, Y., Lejun, Z., Jun, L., Bing, Q., Pirajno, F., Cooke, D.R., 2011. Geological, geochemical characteristics and isotope systematics of the Longqiao iron deposit in the Lu-Zong volcano-sedimentary basin, Middle-Lower Yangtze Changjiang River Valley, Eastern China. Ore Geology Reviews, 43, 154-169.

Taylor, S.R., McLennan, S.M., 1985. The continental crust; its composition and evolution. Oxford, Blackwell, 312pp.

Taylor, H.P., Frechen, J., Degens, E.T., 1967. Oxygen and carbon isotope studies of carbonatites from the Laacher See District, West Germany and the Alnö District, Sweden. Geochimica et Cosmochimica Acta, 31, 407-3.

Torres-Ruiz, J., 2006. Geochemical constraints on the genesis of the Marquesado iron ore deposits, Betic Cordillera, Spain: REE, C, O, and Sr isotope data. Economic Geology, 101, 667-677.

Veizer, J., Hoefs, J., 1976. The nature of O^{18}/O^{16} and C^{13}/C^{12} secular trends in sedimentary carbonate rocks. Geochimica et Cosmochimica Acta, 40, 1387-1395.

Wauschkuhn, A., Ohnsmann, M., Momenzadeh, M., 1984. The Paleozoic rocks of the South Binalud Mountains, NE Iran, an exploration target for Fe, Pb, Zn and Ba. Neues Jahrbuch für Geologie und Mineralogie Abhandlungen, 168, 479-489.

Webb, G.E., Kamber, B.S., 2000. Rare earth elements in Holocene reefal microbialites: a new shallow seawater proxy. Geochimica Cosmochimica Acta, 64, 1557-1565.

Wendt, J., Kaufmann, B., Belka, Z., Farsan, N., Karimi Bavandpur, A., 2005. Devonian/Lower Carboniferous stratigraphy, facies patterns and palaeogeography of Iran. Part II. Northern and central Iran. Acta Geologica Polonica, 55, 31-97.

Wood, S.A., 1990. The aqueous geochemistry of the rare earth elements andyttrium: theorical prediction in hydrothermal solutions to 350ºC at saturation of water vapour pressure. Chemical Geology, 88, 99-125.

Zarei, A., Shafaroudi, A.M., Karimpour, M.H., 2016. Geochemistry and Genesis of Iron-apatite Ore in the Khanlogh Deposit, Eastern Cenozoic Quchan-Sabzevar Magmatic Arc, NE Iran. Acta Geologica Sinica (English Edition), 90, 121-137.

Manuscript received October 2016;
revision accepted December 2017;
published Online April 2018.